Results in Geochemistry 1 (2020) 100004

Contents lists available at ScienceDirect

Results in Geochemistry

journal homepage: www.elsevier.com/locate/ringeo

Petrogenesis of Siletzia: The world's youngest oceanic plateau

T.Jake R. Ciborowski[a,*], Bethan A. Phillips[b,1], Andrew C. Kerr[b], Dan N. Barfod[c], Darren F. Mark[c]

[a] School of Environment and Technology, University of Brighton, Brighton BN2 4GJ, UK
[b] School of Earth and Ocean Science, Cardiff University, Main Building, Park Place, Cardiff CF10 3AT, UK
[c] Natural Environment Research Council Argon Isotope Facility, Scottish Universities Environmental Research Centre, East Kilbride G75 0QF, UK

ARTICLE INFO

Keywords:
Igneous petrology
Geochemistry
Geochemical modelling
Mantle plumes
Oceanic plateau
Large igneous provinces

ABSTRACT

Siletzia is an accreted Palaeocene-Eocene Large Igneous Province, preserved in the northwest United States and southern Vancouver Island. Although previous workers have suggested that components of Siletzia were formed in tectonic settings including back arc basins, island arcs and ocean islands, more recent work has presented evidence for parts of Siletzia to have formed in response to partial melting of a mantle plume. In this paper, we integrate geochemical and geochronological data to investigate the petrogenetic evolution of the province.

The major element geochemistry of the Siletzia lava flows is used to determine the compositions of the primary magmas of the province, as well as the conditions of mantle melting. These primary magmas are compositionally similar to modern Ocean Island and Mid-Ocean Ridge lavas. Geochemical modelling of these magmas indicates they predominantly evolved through fractional crystallisation of olivine, pyroxenes, plagioclase, spinel and apatite in shallow magma chambers, and experienced limited interaction with crustal components.

Further modelling indicates that Siletzia magmatism was derived from anomalously hot mantle, consistent with an origin in a mantle plume. This plume has been suggested to have been the same as that responsible for magmatism within the Yellowstone Plateau. Trace element compositions of the most primitive Siletzia lavas are similar to suites associated with the Yellowstone Mantle Plume, suggesting that the two provinces were derived from compositionally similar sources. Radiogenic isotope systematics for Siletzia consistently overlap with some of the oldest suites of the Yellowstone Magmatic Province. Therefore, we suggest Siletzia and the Yellowstone Mantle Plume are part of the same, evolving mantle plume system.

Our new geochronological data show the province was emplaced during the time when Eocene sea surface temperatures were their highest. The size of Siletzia makes the province a potential contributing factor to the biospheric perturbation observed in the early Eocene.

1. Introduction

Large Igneous Provinces (LIPs) represent large volume (>0.1 Mkm^3; frequently above >1 Mkm^3), mainly mafic (-ultramafic) magmatic events that are not associated with 'normal' tectonic processes such as mid-ocean ridge spreading or subduction (Bryan & Ernst, 2008; Bryan & Ferrari, 2013; Coffin & Eldholm, 1994), and are typically characterised by pulses of magmatism that last a maximum of a few tens of m.y. (Bryan & Ferrari, 2013; Ernst & Bleeker, 2010). In oceanic settings, LIP magmatism often manifests itself as oceanic plateaus that comprise volcanic successions (which may be emplaced both subaerially and subaqueously), a plumbing system of sheets, sills and layered intrusions, and a crustal magmatic underplate (Coffin & Eldholm, 1994; Kerr, 2014; Ernst et al., 2019). Accreted oceanic plateaus are commonly found at convergent pate margins throughout the geological record (Chen et al., 2001; Ichiyama et al., 2014; Kerr, 2014), where their over thickened and relatively buoyant nature has allowed them to resist subduction (e.g., Tetreault & Buiter, 2014).

Most recognised oceanic plateaus are thought to have undergone most of their eruption and emplacement during one main and initial volcanic episode (e.g., Kerr & Mahoney, 2007). For example, a large percentage of the Ontong Java Plateau was erupted over a few million years between ~ 122 Ma and 120 Ma (Chambers et al., 2004; Mahoney et al., 1993), while the majority of the Caribbean Plateau formed at 93–89 Ma (Kerr et al., 2003) and most of the southern Kerguelen plateau at 119–118 Ma (Coffin et al., 2002; Duncan, 2002). In order to be able to generate such quantities of magma over such relatively short periods of

* Corresponding author.
[1] Present address: The Geological Society Publishing House, Brassmill Enterprise Centre, Unit 7, Brassmill Lane, Bath, BA1 3JN, UK.

https://doi.org/10.1016/j.ringeo.2020.100004
Received 23 December 2019; Received in revised form 9 October 2020; Accepted 26 October 2020

geological time, the source region is required to be fundamentally different to the ambient mantle, i.e. it must be either, hotter, more fertile, more volatile rich, or some combination of these factors (e.g., Campbell & Griffiths, 1990; Kerr, 2014). It has been determined that decompression partial melting of a dominantly peridotite mantle source with a higher than ambient T_P (potential temperature, that is the temperature mantle material would have were it adiabatically decompressed to the surface of the earth (McKenzie & Bickle, 1988)) can produce the magmatic activity that characterise oceanic plateaus (Fitton & Godard, 2004; Herzberg, 2004; Herzberg et al., 2007; Putirka, 2008).

Therefore, the mantle plume paradigm is currently the preferred genetic mechanism for the majority of LIPs (including oceanic plateaus) observed in the geological record (see reviews in Campbell, 2007; Kerr & Mahoney, 2007 and Ernst, 2014). The model predicts that the high volumes of magmatism associated with LIPs occurs in response to the melting (via decompression) of a cylindrical zone of anomalously hot mantle material, upwelling from significant depths in the mantle (Campbell & Griffiths, 1990). The mantle plume model for LIPs is particularly relevant to those emplaced during the Cenozoic where seismic tomography has frequently detected anomalously low-velocity (presumably high temperature) regions in the mantle beneath the focus of surface volcanism downwards to some boundary layer within the mantle (Campbell, 2007; Montelli et al., 2006; Wolfe et al., 1997).

In this contribution, we present 271 new whole-rock geochemical analyses from the Siletz Terrane (12 major element oxides and 33 trace elements). These analyses span each constituent suite of the Siletz Terrane, and crucially, represent the first consistent data set analysed by a single laboratory, for the entire magmatic system. We use these geochemical data to assess the petrogenesis of Siletzia, an accreted oceanic plateau composed of the constituent suites of the Siletz Terrane and the Grays River Volcanics, which together, are preserved in the Cascadia forearc region of Vancouver Island, Washington and Oregon in North America (Fig. 1).

Aside from their petrological implications, it is important to understand the evolution of oceanic plateaus because the large volume eruptions over small time periods have environmental consequences (e.g., Kerr, 2005). Therefore, we also present 9 new Ar–Ar ages which further constrain the timing and duration of the Siletzia magmatism, and its potential relationship to the Palaeocene-Eocene Thermal Maximum (PETM).

Interpreted tectonic settings for Siletzia magmatic suites are varied. It has been argued that some of the mafic suites represent accreted island chains initially formed via hotspot volcanism (Duncan, 1982), which itself may have been the initial manifestations of the Yellowstone plume (Haeussler et al., 2003; Pyle et al., 2009; Wells et al., 2014). In contrast, others have suggested Siletzia was emplaced in a rift-related marginal basin (Brandon, 2014; Wells et al., 1984), or formed by passive mantle upwelling through a slab window during subduction of a mid-ocean ridge (e.g., Babcock et al., 1992).

The new dataset presented here is used to assess the petrogenetic evolution of Siletzia and its constituent formations. In this paper we investigate the nature of the mantle sources and melting regime which produced the primary magmas of the province and use geochemical modelling to constrain the evolution of these primary magmas during their residence in the crust. A potential petrogenetic link between Siletzia and the Yellowstone Magmatic Province is explored, before, finally, we assess the potential effect the formation of Siletzia had on the biosphere.

2. Overview of Siletzia

2.1. Siletz terrane

The Siletz terrane represents an oceanic terrane which was accreted to western North America shortly after its formation in the Eocene (Duncan, 1982; McCrory & Wilson, 2013; Snavely et al., 1968). The terrane is composed of 2.6×10^6 km^3 of predominately mafic pillow lavas, intrusions and subaerial flows (Phillips et al., 2017; Trehu et al., 1994) which are preserved in three formations (Fig. 1). The first of these is the Siletz River Volcanic Formation, which is found in Oregon and crops out near Tillamook and Roseburg. The lavas are mostly comprised of aphyric pillow basalts and massive flows which are interbedded with cherts, turbidites and siltstones (Phillips et al., 2017; Snavely et al., 1968). The presence of tuffaceous flows, lapilli-rich horizons and oxidised flow tops indicate that part of the volcanic activity was subaerial (Phillips et al., 2017; Snavely et al., 1968).

The second formation is the Crescent Formation which crops out in the Olympic Mountains and Willapa Hills of southern Washington (Fig. 1) and is subdivided into a lower (mostly subaerial) unit and upper (mostly submarine) unit. The lower unit is dominated by pillow basalts with minor massive flows and basaltic breccias that conformably overlie siliciclastic submarine sequences (Babcock et al., 1992) while the upper unit is primarily composed of massive basaltic flows, the tops of which are partially oxidised (Babcock et al., 1992; Glassley, 1974).

The third formation is the Metchosin Igneous Complex which is limited in outcrop to the southern tip of Vancouver Island and consists of a lower unit comprising sheeted dykes, pillow basalts, massive flows and an overlying ~1000 m thick upper unit of subaerial massive sheet flows and lesser tuffs and basalt breccias (Phillips et al., 2017). A number of gabbroic and dolerite bodies intrude all levels of the volcanic stratigraphy of the Metchosin Igneous Complex (Timpa et al., 2005).

Detailed petrographic analysis carried out by Phillips et al. (2017) shows that the mineralogy of the mafic rocks is dominated by plagioclase, clinopyroxene and Fe–Ti oxide. The Siletz River Volcanics are the only Siletz Terrane rocks to contain abundant olivine (and pseudomorphs after olivine), while elsewhere, ophitic textures are common. Sub-solidus alteration of the Siletz Terrane rocks is limited, with the Crescent Formation and Siletz River Volcanics only characterised by zeolite to prehnite–pumpellyite facies assemblages. An exception to this is the Metchosin Igneous Complex and some Crescent Formation outcrops which display up to greenschist-facies alteration assemblages. Argon–Argon (Ar–Ar) and Potassium–Argon (K–Ar) has dated the igneous activity of the Siletz Terrane to have occurred between 56-49 Ma (Duncan, 1982; Moothart, 1993). Recent work using U-Pb dating (Eddy et al., 2017) has yielded ages of 51.2–50.9 Ma and 53.4–48.1 Ma for the Metchosin Igneous Complex and Crescent Formation respectively, while Haeussler et al. (2003), has reported U-Pb ages of 53–50 Ma for the Siletz River Volcanic Formation.

Previous workers have shown that the Siletz Terrane lavas contain up to 15 wt. % MgO, with whole-rock major element compositions which range from picritic to rhyolitic (Appendix 1). The trace element signatures of the Siletz Terrane lavas are similarly varied, as shown by the Crescent Formation and Siletz River Volcanics which show moderate to extreme enrichments in the most incompatible elements relative to the least incompatible. The compositions are similar to those observed in modern day hotspot-related ocean island basalts (Phillips et al., 2017; Rarey, 1985). In contrast, the basalts of the Metchosin Igneous Complex, Timpa et al. (2005) and Phillips et al. (2017) show trace element signatures characterised by depletions in the most incompatible elements relative to the least incompatible trace elements, and have compositions similar to modern day mid-ocean ridge basalts.

A plume source for the Siletz Terrane has been proposed by Pyle et al. (2009, 2015), on the basis of Sr, Pb and Nd isotopic compositions which they argue are indistinguishable from parts of the Columbia River Basalt (CRB) Province - itself widely considered to be related to the Yellowstone mantle plume (Brandon & Goles, 1988; Geist et al., 2002; Prestvik & Goles, 1985). This isotopic similarity is used as evidence of a probable cogenetic link between the Siletz Terrane and the CRB, with the Siletz Terrane representing melting of the nascent Yellowstone plume head, and the basalts of the CRB related to melting of the plume tail. However, more recent published isotopic analysis by Phillips et al. (2017), reveals clear isotopic differences between the Siletz Terrane and the CRB that

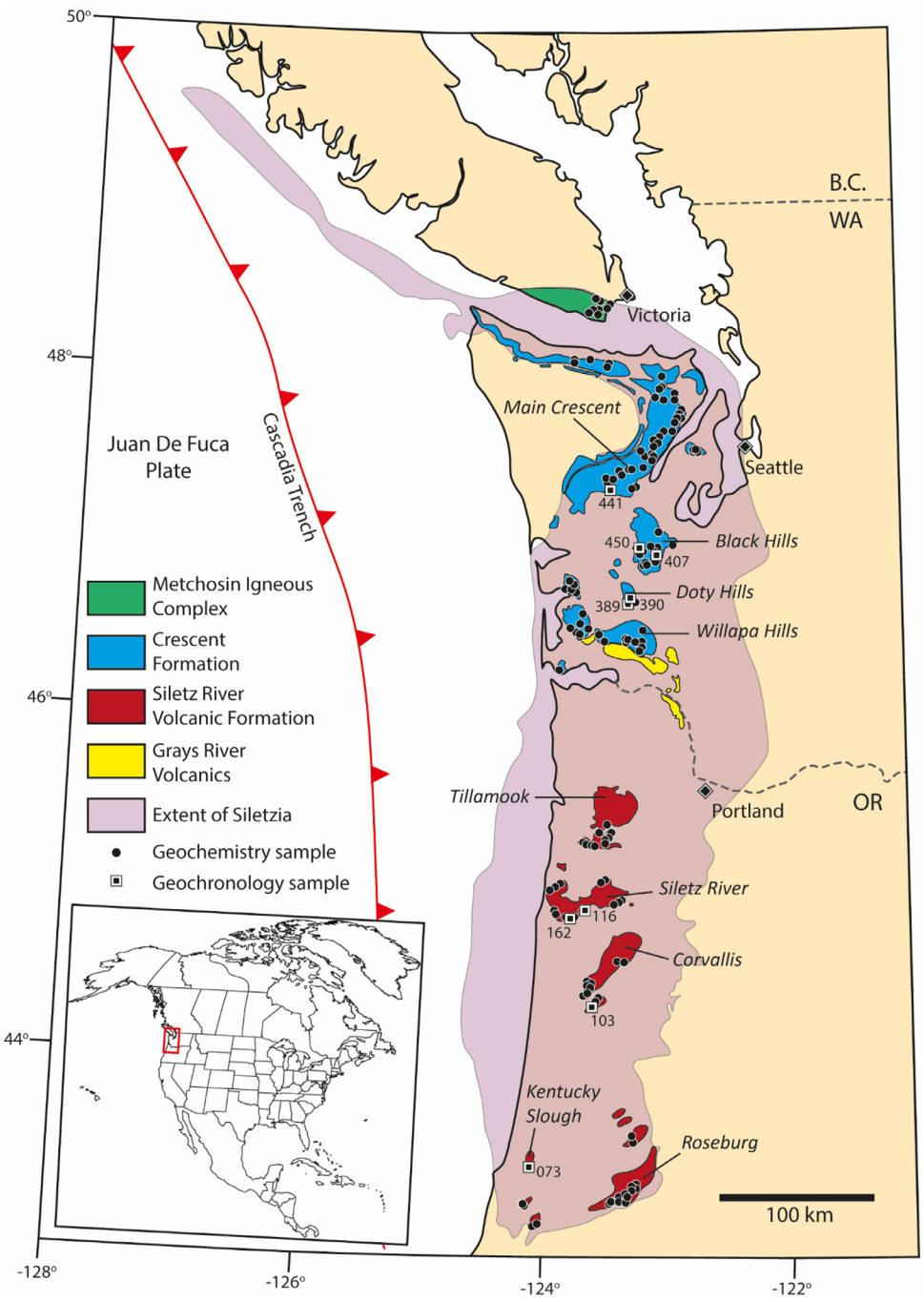

Fig. 1. Map showing the distribution of the consistent suites comprising Siletzia (modified after Phillips et al., (2017) and McCory & Wilson (2013)). Also shown are the locations of samples collected by this study for geochemical and geochronological analysis. Full sample location data available in Appendix 1.

are difficult to reconcile with a cogenetic origin for both the Siletz Terrane and CRB. Instead, Phillips et al. (2017) suggest that the variable Siletz Terrane trace element geochemistry and isotopic compositions that fall on mixing trends between HIMU, EM2 and depleted mantle reservoirs show that the Siletz magmatism is derived from a compositionally heterogeneous deep plume source, distinct from the source of the CRB.

2.2. Grays river volcanics

The Grays River Volcanics consist of a ~3500 m thick pile of lava flows, volcanoclastic rocks and interbedded sedimentary rocks, preserved within the Coast Range basalt province (McCutcheon, 2003). The volcanic rocks comprise an upper and lower unit (Kleibacker, 2001), with the lower unit being dominated by pillow basalts and hyaloclastites, while the upper unit is made up of subaerially erupted basaltic andesites and dacites. Ar–Ar dating reveals that the entirety of the Grays River Volcanics was emplaced between 40.1 and 36.8 Ma, with the lower basaltic unit emplaced between 40.1 and 39.0 Ma (Kleibacker, 2001).

Previous geochemical analyses of the Grays River Volcanics show that the basalts of the lower unit are tholeiitic, range in MgO from 2.7 to 9.5 wt. %, and are characterised by a moderate enrichment in the Light Rare Earth Elements (LREE) relative to the Heavy Rare Earth Elements (HREE) and incompatible element enrichments similar to ocean island basalts (Chan et al., 2012; Phillips et al., 1989). Aside from these trace element signatures, Chan et al. (2012) suggests that the low B/Be ratios and high $^{206}Pb/^{204}Pb$ ratios recorded by the Grays River Vol-

canics are most likely to have been caused by partial melting of a deep mantle plume source that incorporated lesser amounts of depleted mantle components. Chan et al. (2012) and Pyle et al. (2009) propose that the Grays River Volcanics were derived from the nascent Yellowstone plume, which supplied the primary magmas of the suite.

3. Analytical methods

3.1. Major elements and trace elements

Rock sample preparation and geochemical analysis was carried out at Cardiff University. Weathered surfaces, veins and alteration patches were removed from the rock samples using a diamond-bladed rock saw. Samples were then crushed to a coarse grit by a steel jaw crusher. Approximately 80 ml of each sample was reduced to a fine powder in an agate ball mill. Afterwards, approximately 2 g of each powdered sample was ignited for two hours in a furnace at 900 °C to drive off volatile substances and determine loss on ignition (LOI) values.

Samples in this study were prepared for Inductively Coupled Plasma (ICP) analysis using the lithium metaborate fusion method. To prepare the samples, 0.1 ± 0.001 g of each ignited sample was mixed with 0.6 ± 0.004 g of lithium metaborate flux in a platinum crucible. A few drops of lithium iodide wetting agent were added to each mixture which was then fused (at approximately 1000 °C) using the Claisse Fluxy automated fusion system. After the mixture was then dissolved in a 50 ml solution of 4% HNO_3. After the mixture had fully dissolved, 1 ml of 100 ppm Rh spike was added to the solution which was then made up to 100 ml with 18.2 Ω deionised water obtained using a Milli-Q ® purification system. Approximately 20 ml of each solution was run on ICP-Optical Emission Spectrometry (OES) to obtain major element and some trace element abundances. An aliquot of 1 ml of each solution was added to 1 ml of In and Tl and 8 ml of 2% HNO_3 and run on the ICP-Mass Spectrometer (MS) to obtain trace element abundances. The instruments at Cardiff University used to analyse elemental compositions are a Jobin Yvon Horiba Ultima 2 ICP-OES and a Thermo Elemental X7 series ICP-MS. Full analytical results including repeat runs of standard basalt JB-1A and analyses of other international reference materials, can be found in Appendix 1. The vast majority of elements are within 2 standard deviations (σ) of certified values and those that are not in this range (e.g., Ni and Cu) are not included in the discussion.

3.2. Geochronology

Plagioclase separates were initially collected from samples via magnetic separation, followed by light leaching in nitric acid and hand picking. These separates and neutron flux monitors were placed in Cu or Al foil packets and stacked in quartz tubes. The relative positions of the packets were carefully measured for later reconstruction of neutron flux gradients. The sample package was irradiated in the McMaster University, Canada reactor, Cd-shielded facility. Fish Canyon Sanidine (FCs, 28.294 ± 0.036 Ma, Renne et al., 2011) was used to monitor ^{39}Ar production and establish neutron flux values (J) for the samples.

Gas was extracted from samples using an all-metal resistively-heated furnace with multi-step heating schedules ranging from ~700 to 1500 °C. Liberated argon was purified of active gases (e.g, CO_2, H_2O, H_2, N_2, CH_4) using three Zr–Ti–Al getters; one at 25 °C and two at 400 °C. Data were collected on a GVi instruments ARGUS 5-collector mass spectrometer using a variable sensitivity faraday collector array in static collection (non-peak hopping) mode (Mark et al., 2009; Sparks et al., 2008). Time-intensity data were regressed to t_0 with second-order polynomial fits to the data. Mass discrimination was monitored by comparison to running-average values of an air standard. Typical average total system blank for furnace extractions, measured between each sample run, are 2×10^{-15} mol ^{40}Ar, 2×10^{-17} mol ^{39}Ar, 3×10^{-17} mol ^{36}Ar over the temperature range where age information is extracted; these blank levels yielded average sample/blank ratios ranging from 10 to 2000. All data are blank and mass discrimination corrected. Plateaus are calculated with contiguous steps (minimum 5 steps and 50% ^{39}Ar released), indistinguishable in age at 2σ uncertainty. Inverse isochrons are calculated with concordant plateau steps and used to test that trapped components are indistinguishable from the composition of modern air and that resultant age is indistinguishable from the plateau age at 2σ uncertainty.

4. Results

4.1. Geochemistry

The 271 new whole-rock major and trace element geochemical analyses presented here represent the single most extensive sampling of the Siletz Terrane to date, both in terms of geographic distribution and number of samples analysed. These new high-quality data have been integrated with older data from the literature, to facilitate for the first time, an assessment of the magmatic evolution of Siletzia as a whole. A representative selection of our new data, including the first trace element data collected from the basalts of the Siletz River Formation, are summarised in Table 1 and given in full in Appendix 1. Also included in Appendix 1 are the 493 individual whole-rock analyses from the constituent suites of the province reported by previous workers.

The total alkali vs. silica (TAS) diagram (LeBas et al., 1986) classifies the Siletzia samples as a continuum of predominantly tholeiitic picrobasalts, basalts, basaltic andesites, andesites and dacites and rhyolites (Fig. 2A), with far fewer analyses plotting in the alkaline basalt, phono-tephrite and other regions. On the Zr/Ti vs Nb/Y diagram (Pearce, 1996), which is less susceptible to sub-solidus elemental mobility at greenschist facies, exhibited by some of the Siletz samples (Phillips et al., 2017), the majority of the Siletzia samples plot as an overlapping array between the basalt and alkali basalt field. On this diagram, only a small minority of samples from the Siletz River and Crescent Formations falling on trends towards rhyolitic and tephriphonolitic compositions (Fig. 2B). The new samples we present here tend to be more mafic than the literature analyses. This is a product of our sampling strategy which aimed to acquire more primitive samples that would better record mantle source characteristics.

Our new data, taken together with the published data, show that the most magnesian rocks of Siletzia belong to the Crescent Formation, which contain up to 15 wt. % MgO. The most magnesian lavas of the Siletz River formation contain ~14 wt. % MgO, while the most magnesian samples from the Metchosin Igneous Complex and Grays River Volcanics contain ~11 wt. % MgO and ~10 wt. % MgO respectively.

All suites show consistently increasing SiO_2, Na_2O and K_2O with decreasing MgO, while CaO shows a uniform decrease with decreasing MgO. Al_2O_3 shows no obvious correlation with MgO (Fig. 3). $FeO_{(T)}$ trends for the province are harder to characterise, but seem to record a point of inflection whereby samples with > 4 wt. % MgO, record decreasing $FeO_{(T)}$ with increasing MgO, while samples with < 4 wt. % MgO record decreasing $FeO_{(T)}$ with decreasing MgO. These trends are widely interpreted (e.g., Peterson & Moore, 1984) to be the result of the initial fractionation of olivine, clinopyroxene and plagioclase from basaltic parent magmas, followed by subsequent fractionation of Fe–Ti oxides. This potential fractionation history is in agreement with published petrographic analyses (Phillips et al., 2017) which shows that the mineralogy of the mafic rocks of the Siletz Terrane (as focussed on here) is dominated by plagioclase, clinopyroxene and Fe–Ti oxide.

Although the major element bivariate trends are diffuse, this relative scatter cannot be ascribed to element remobilisation during metamorphism, which, for the Siletzia suites is of insufficient grade to have remobilised many of the elements displayed in Fig. 3 (Phillips et al., 2017). Instead, it is likely that some of this apparent scatter within the suites, is the result of their derivation from multiple parent magmas, potentially each with its own subtly different melting and fractionation history. This might be indicated by the bivariate plots involving MgO and CaO and

Table 1
Summary of the key geochemical ranges for the constituent suites of Siletzia. n denotes number of samples each range is defined by. Full data available in electronic appendix.

	Metchosin Igneous Complex	Siletz River Volcanic Formation	Crescent Formation	Grays River Volcanics
Age (Ma)	51.08	50.47	50.77	39.10
+ / - (Ma)	0.16	3.00	2.64	2.30
n	81	225	332	126
MgO (wt. %)	4.60–11.19	0.12–13.81	0.53 - 15.12	2.27–9.53
$FeO_{(T)}$ (wt. %)	4.06–15.04	2.65–15.87	3.07 - 20.85	7.78–14.15
SiO_2 (wt. %)	45.10–54.33	37.20–71.41	41.47 - 70.37	45.66–62.18
Ni (ppm)	40–1002	6–1245	1 - 1219	9–167
Cr (ppm)	60–1012	5–367	1 - 590	2–375
La/Sm	0.66–1.87	1.65–13.53	0.48 - 4.78	1.37–4.78
Gd/Yb	1.06–1.67	1.44–14.12	0.96 - 3.41	2.35–3.57
Nb/Th	4.97–31.70	0.79–25.34	1.73 - 173.00	8.69–21.09
$^{87}Sr/^{86}Sr$	0.703110–0.703880	0.703056–0.703553	0.703077 - 0.705287	0.703068–0.703548
$^{143}Nd/^{144}Nd$	0.51293–0.51312	0.512877–0.513035	0.512651 - 0.513058	0.512896–0.512986
$^{206}Pb/^{204}Pb$	18.7884–19.0965	18.9291–19.8567	18.7681–19.4409	18.947–19.525
$^{207}Pb/^{204}Pb$	15.5091–15.5362	15.5356–15.6173	15.5224–15.6247	15.536–15.603
$^{208}Pb/^{204}Pb$	38.3307–38.7082	38.5914–39.4752	38.475–39.1266	38.511–39.23
$^{176}Hf/^{177}Hf$	0.283168–0.283196	0.28302–0.283111	0.282892–0.283175	-

Na_2O which appear to show evidence of a bifurcation of trends in the Crescent Formation and Snake River Volcanics (highlighted on Fig. 3C and F). As will be investigated in more detail later, this may indicate that these suites are actually composite suites made up of the products of multiple magmatic systems which experienced different petrogenetic histories.

All of the Siletzia suites show positive correlations between MgO and elements that are compatible during normal basaltic differentiation such as Cr, Ni and Sc (Fig. 4). Incompatible element (La, Sm, Y, Nb) vs. MgO trends all record negative correlations, but for the Siletz River and Crescent Formations, the data show a large degree of scatter, with several samples plotting outside of the main trends defined by the bulk of the samples. Incompatible element vs. Zr trends (Fig. 5) show a similar pattern. Samples from the Grays River Volcanics and Metchosin Igneous Complex plot on linear arrays, while a number of samples from the Siletz River and Crescent formation plot as a diffuse scatter away from the main trend. It is unlikely that this scattering is the result of elemental remobilisation during metamorphism of the Crescent and Siletz River formations as the prehnite-pumpellyite-greenschist metamorphic grade for these suites (Phillips et al., 2017) is usually insufficient to have remobilised the high field strength elements, including the Rare Earth Elements (Pearce, 1996). Instead, the scatter observed in Fig. 5 for the Crescent and Siletz River formations is potentially due to the formations being derived from a number of primary magmas, which is consistent with the bifurcation of major element trends highlighted in Fig. 3C and Fig. 3F.

The incompatible trace element systematics of the Siletzia suites vary between the constituent suites. The majority of samples from the Siletz River, Crescent Formation and Grays River Volcanics plot as overlapping clusters similar in composition to Oceanic Plateau Basalts (Fig. 6). Fewer samples from these three suites classify as Oceanic Island Basalts according the scheme of Condie (2005), while only several samples from each classify as Mid Ocean Ridge or Volcanic Arc Basalts. Using the same classification, the Grays River Volcanics show a slightly smaller compositional variability, plotting almost entirely as Oceanic Island Basalts. According to the scheme of Pearce (2008), the vast majority of samples plot within the mantle array between Normal Mid Ocean Ridge and Ocean Island Basalts. Only very few samples from the Crescent Formation and Siletz River Volcanics plot on vectors towards Upper Continental Crust, which may indicate that contamination processes operated during the petrogenesis of some of these suites.

4.2. Geochronology

In total, 14 basalt samples were selected for Ar–Ar dating on the basis of petrographic freshness. Of these samples, 8 yielded acceptable step-heating plateau ages. All ages were obtained on plagioclase separates except sample 116 for which the age was obtained from the groundmass. These data are discussed below, summarised in Table 2 and the step-heating plateau experiments and isochron plots are given in Appendix 2.

Sample 450, from the Black Hills Group, yielded an Ar–Ar plateau age of 34.16 ± 0.40 Ma which is younger than the 56–51 Ma K–Ar reported by Duncan (1982). This sample is tholeiitic and similar in elemental and isotopic composition to other basalts of the Siletz terrane (Phillips et al., 2017). This age is similar to those from the Cascade Head Volcanics to the south that have been dated to 34.2 Ma (Ar–Ar whole rock plateau, Wells et al., 2014) and the Upper Grays River Volcanics at 36.8 ± 0.5 Ma. Hirsch and Babcock (2009) also note a similar age for a sample further to the north, yielding an Ar–Ar plateau age of 31.2± 0.2 Ma, originally thought to be correlated with the Crescent Fm.

Basalt sample 441 is from near the base of the upper Crescent Formation in the south of the Main Crescent sequence and has been determined to have an Ar–Ar plateau age of 55.96 ± 0.92 Ma. This age is indistinguishable from published whole rock $^{40}Ar/^{39}Ar$ ages for these basalts of 51.0 ± 4.7 Ma (Hirsch & Babcock, 2009), but slightly older than calcareous nanoplankton ages of 53.5–49 Ma, determined for interbedded marine mudstones (Bukry & Snavely, 1988).

Samples 390 and 389 from the Doty Hills Group of basalts, part of the Crescent formation in southern Washington, yield Ar–Ar plateau ages of 47.62 ± 0.28 and 49.49 ± 0.40 Ma respectively. While there are no published ages for this particular region of the Crescent Formation, the Willapa Hills area ~ 15 km to the south have $^{40}Ar/^{39}Ar$ ages ranging from ~54 Ma (at the base of the lava sequence) to 48.7 ± 0.5 Ma (at the top of the lava sequence) (Duncan, 1982; Wells et al., 2014) suggesting that the Doty Hills basalts are correlative with late stage Crescent Fm. in this region.

Sample 116 is a basalt from the Siletz River type locality in Oregon and has an Ar–Ar plateau age of 53.35 ± 0.24 Ma. This is similar to the published ages of 53.5–49 Ma (coccolith zones CP10 and CP11) (Bukry & Snavely, 1988) and 53.3–49.5 Ma ($^{40}Ar/^{39}Ar$ step heating ages) (reported by Pyle et al., 2009). Sample 162, a similar basalt from the Siletz River Formation type locality, has yielded an Ar–Ar plateau age of 58.84 ± 5.21 Ma which is nearly indistinguishable from sample 116 and the ages reported by Pyle et al. (2009).

Basalt sample 103 from the Corvallis area, Oregon is part of the Siletz River Volcanic Formation. While there are no specific ages available for the Corvallis area, the ages are likely to be similar to those discussed above for the Siletz River type locality. The Ar–Ar plateau age determined for this sample is 51.48 ± 0.48 Ma, which is again consistent with the published ages.

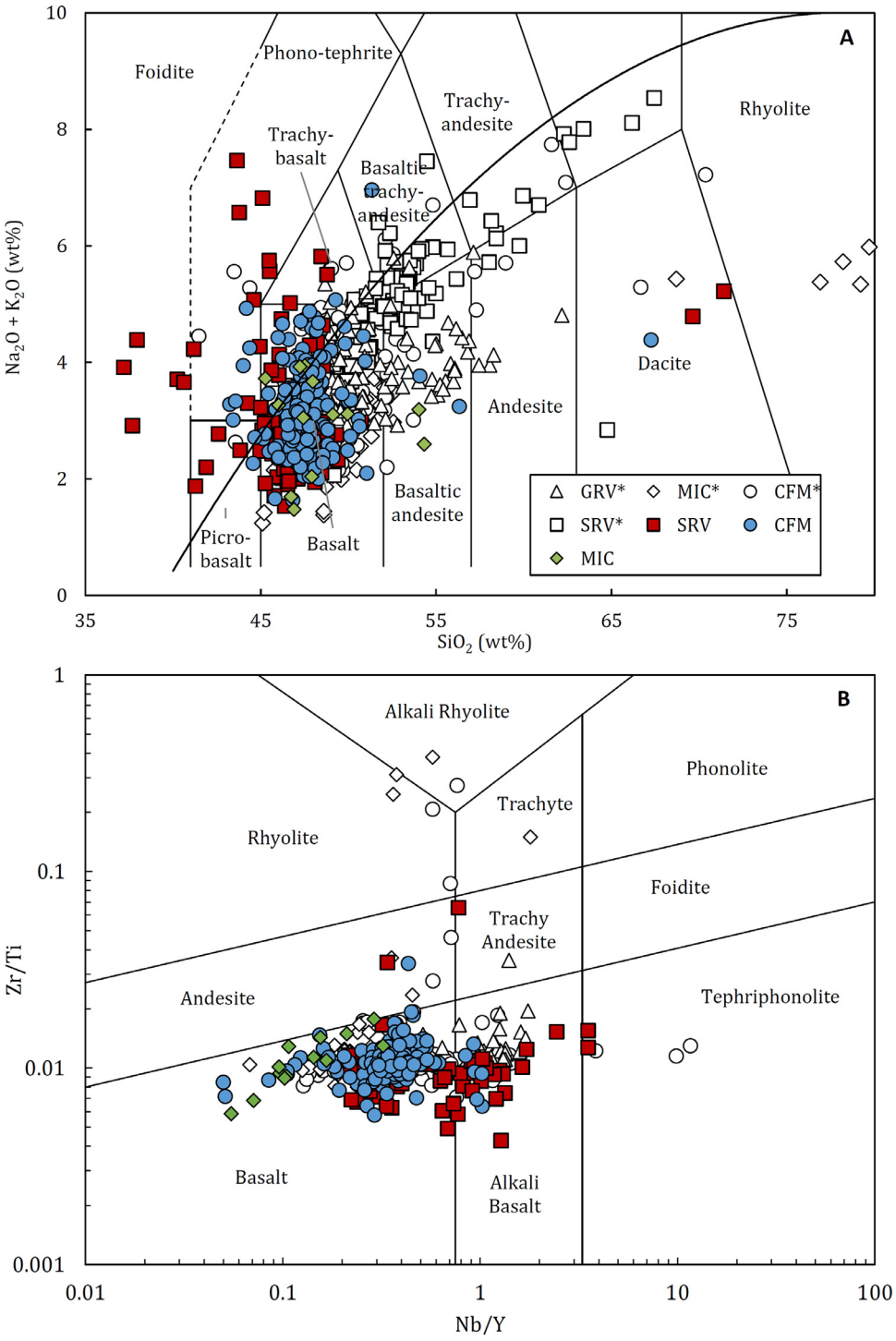

Fig. 2. Chemical classification of the Siletzia samples (electronic appendix) using the TAS diagram (LeBas et al., 1986) with data calculated on 100% anhydrous basis – A, and the Zr/Ti vs. Nb.Yb diagram (Pearce, 1996) – B. Alkaline-Tholeiite line in A from Irvine & Baragar (1971). GRV – Grays River Volcanics, MIC – Metchosin Igneous Complex, CFM – Crescent Formation, SRV – Siletz River Volcanic Formation. * denotes data sourced from literature. Coloured symbols denote new data. White symbols are literature data. Coloured symbols are new data.

Finally, sample 073 is a phyric basalt from the Kentucky Slough Group in southern Oregon and is classified as part of the Roseburg area of the Siletz River Formation in this study. While there are no specific ages published for this Group, the basalts in the Roseburg Group have been dated to be between 56 and 53.3 Ma ($^{40}Ar/^{39}Ar$ and calcareous nanoplankton) (Pyle et al., 2009). The Ar–Ar plateau age for this sample is 48.55 ± 0.29 Ma, which is significantly younger than those of the Roseburg basalts, but consistent with our younger ages in northern parts of the terrane, e.g., samples 389 and 390, Grays River Volcanics analyses in Duncan (1982), and a dolerite from Willapa Hills with an Ar–Ar plateau of 48.7 ± 0.5 Ma (Wells et al. 2014).

5. Geochemical selection and screening

Petrogenetic modelling software can be used to calculate primary magma compositions, which could feasibly fractionate to form an observed lava composition. One such piece of software, PRIMELT3 (Herzberg & Asimow, 2015) incrementally adds or subtracts olivine from an observed lava composition, while simultaneously modelling melting of fertile mantle peridotite. This hybrid forward and inverse modelling (which assumes olivine is the only phase to have fractionated from the magma) continues until PRIMELT3 computes a melt fraction capable of: (1) being formed by partial melting of mantle peridotite,

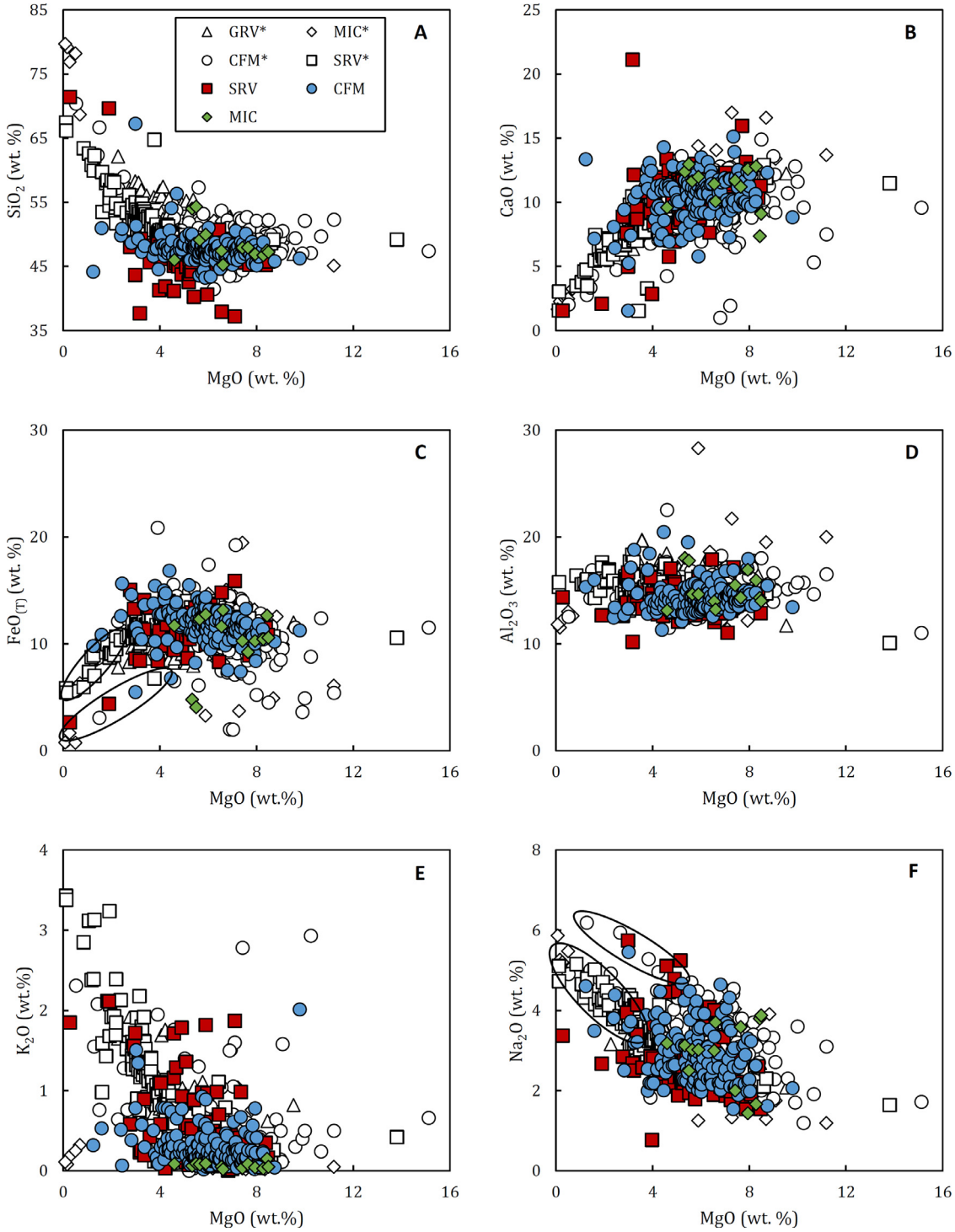

Fig. 3. Representative major element vs. MgO bivariate diagrams of the Siletzia samples. Highlighted are the potential bifurcation of trends in C and F. White symbols are literature data. Coloured symbols are new data. Full data in Appendix 1.

and; (2) replicating the major element composition of the observed lava through the accumulation or fractionation of olivine. In addition, PRIMELT3 also calculates the degree of partial melting (by both batch and accumulated-fractional melting), the temperature of the olivine liquidus, the olivine composition in equilibrium with the primary magma, the amount of olivine required to fractionate from/accumulate within the primary magma in order to form the observed lava composition, and the mantle potential temperature (T_P) required to generate the primary magma.

Although PRIMELT3 is designed to identify samples – particularly those with more evolved compositions – that are unsuitable for the program, datasets must first be filtered to remove evolved samples which may yield spurious thermobarometric results (Herzberg & Asimow, 2008, 2015). Most LIP magmas, by the time they are erupted or intruded, have experienced significant fractional crystallisation (e.g., Hartley & Thordarson, 2009 and Kerr & Mahoney, 2007) and Siletzia is no exception. As shown in the previous section, the vast majority of the lavas sampled from Siletzia contain between 4 and 10 wt. % MgO and

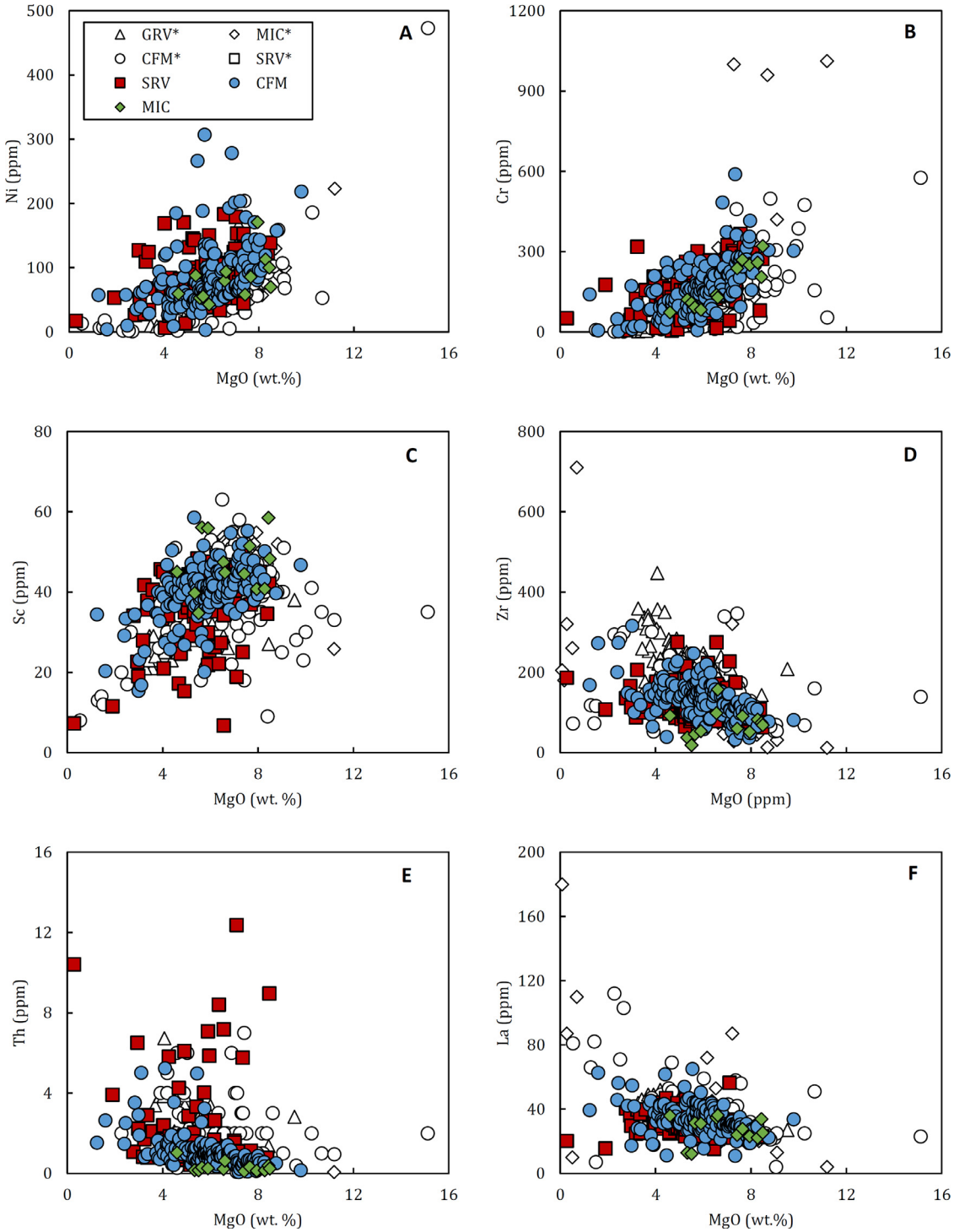

Fig. 4. Trace element vs. MgO bivariate diagrams of the Siletzia samples. White symbols are literature data. Coloured symbols are new data. Full data in Appendix 1.

so many will have undergone significant fractionation of phases other than olivine and Cr-spinel (e.g., clinopyroxene and plagioclase). Thus, the Siletzia database must be carefully screened prior to modelling. To screen our initial dataset (n = 778) we first removed all samples with <7.5 wt. % MgO [which are likely to have experienced clinopyroxene fractionation (Herzberg & Asimow, 2008)], or those which fall outside of olivine control lines on major element bivariate diagrams (Fig. 3). Of the 100 analyses left following this filtering, 28 gave permissible PRIMELT3 melting solutions through either batch or accumulated fractional melting models (Table 3). These samples include representatives from each of the constituent formations of Siletzia and their geochemical data are detailed in Table 4.

6. Discussion

6.1. Primary magmas

The major element composition of the primary magmas computed by PRIMELT3 for the 28 Siletzia samples are shown in (Table 3). PRIMELT3

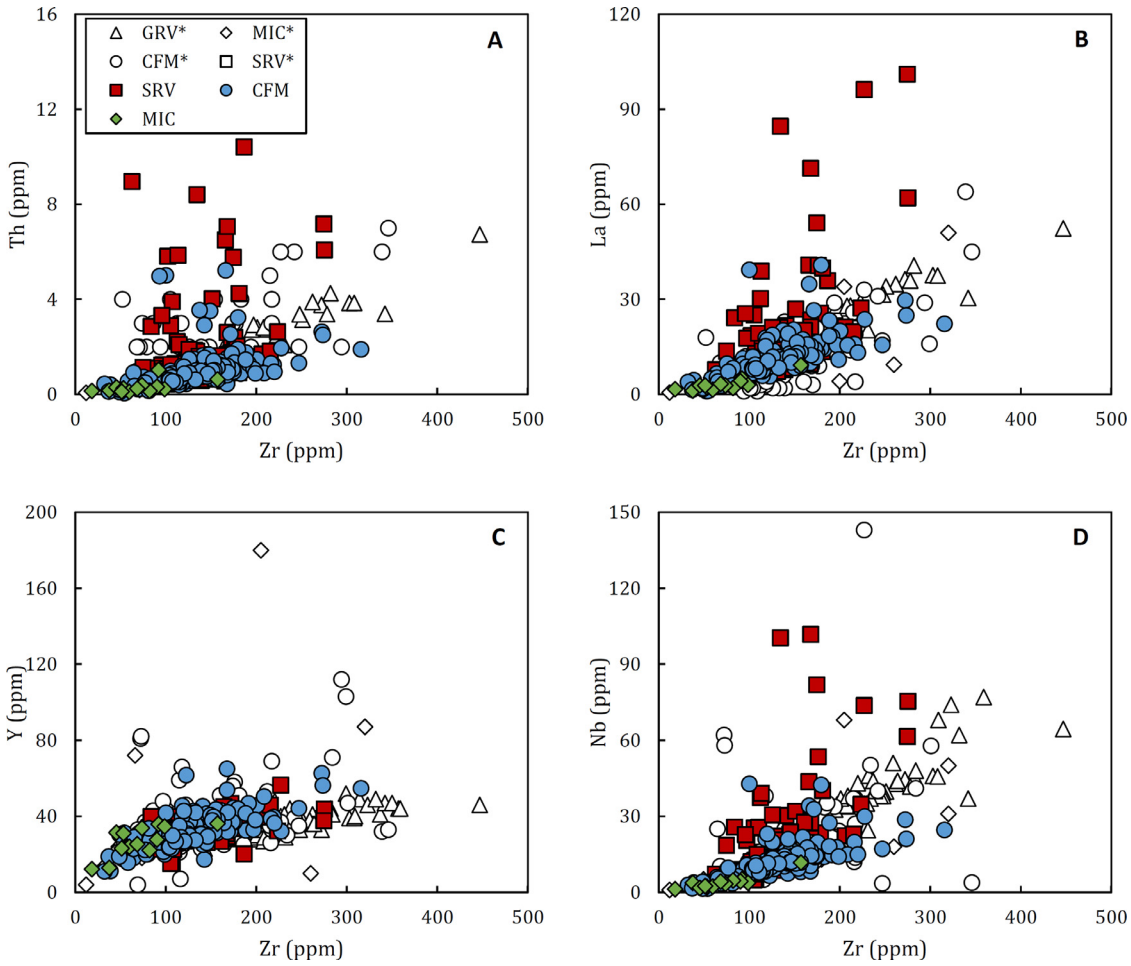

Fig. 5. Trace element vs. Zr bivariate diagrams of the Siletzia samples. White symbols are literature data. Coloured symbols are new data. Full data in Appendix 1.

does not calculate trace element abundances in the computed primary magmas. However, using the equation for Rayleigh fractional crystallisation (Eq. 1) in conjunction with the estimates of olivine fractionation (Table 3) from PRIMELT3 can yield primary magma trace element compositions (Hastie et al., 2016).

$$C_0 = \frac{C_l}{F^{(D_{ol}-1)}} \quad (1)$$

Where C_0 is the concentration of the trace in the primary magma, C_l is the concentration of the trace element in the sample, F is the degree of melt remaining (after olivine fractionation – as calculated by PRIMELT3), and D_{ol} is the olivine mineral/melt partition coefficient of the trace element during olivine fractionation (taken from Bédard, 2001). The calculated trace compositions of the primary magmas are shown in Table 5.

The primary magmas calculated for the Siletz River Formation and Grays River Volcanics have similar trace element signatures which are characterised by enrichments in the most incompatible trace elements relative to the least incompatible trace elements, e.g., $(La/Yb)_N > 1$, and depleted HREE patterns. Both of these primary magmas have trace element compositions intermediate between EMORB and OIB, though the LREE systematics of the Siletz River Primary magma are more similar to OIB than the Grays River Volcanics primary magma (Fig. 7A and 7B).

The primary magmas of the Metchosin Igneous complex (Fig. 7C) all have trace element signatures very similar to NMORB in that they all show depletions in the most incompatible elements relative to the least incompatible elements.

Arguably, the most compositionally complex primary magmas belong to the Crescent Formation. Two (potentially three) primary magma types can be discerned from the primary magma compositions of PRIMELT3-successful Crescent Formation samples. Group 1 primary magmas (Fig. 7D) have trace element patterns virtually identical to EMORB, characterised by enrichments in the most incompatible elements relative to the least incompatible elements, $(La/Yb)_N > 1$ and $(Nb/La)_N > 1$. Group 2 primary magmas (Fig. 7E) are characterised by depletions in the most incompatible elements relative to the least incompatible elements, $(Gd/Yb)_N \sim 1$ and $(Nb/La)_N > 1$. A third group (Fig. 7F) of Crescent Formation primary magmas, calculated from analyses of Babcock et al. (1992) and Glassley (1974) might be delineated on the basis of $(Th/Nb)_N$ ratios > 1, which set these samples apart from the other primary magmas calculated here. However, the analyses from these older papers do not contain the full trace element suite in the primary data. Thus, a full description of their primary magma trace element geochemistry is impossible, and thus, further investigation of their petrogenesis will be limited in this study.

The extent of melting and olivine fractionation calculated by PRIMELT3 for all samples shows large overlap between constituent suites (Table 3). This means that the differences in the trace element signatures of the primary magmas for each suite can only be explained due to their derivation from compositionally distinct mantle sources. The nature of these mantle sources will be explored later.

6.2. Magmatic evolution

This section assesses how each of the constituent Siletzia suites evolved to produce the compositional variation observed in the analysed lavas (Fig. 2). MELTS_Excel (MELTS) is thermodynamic modelling

Table 2
Summary of the Ar–Ar ages successfully calculated for the 9 Siletzia samples. Notes: Samples were irradiated in the McMaster University reactor, Cd-shielded facility. Fish Canyon sanidine (28.294 ± 0.036 (1σ) Ma, Renne et al., 2011) was used to establish neutron flux values (J). Decay constants are listed in Renne et al. (2011). A: analytical error only. F: full external error including decay constant and standard age uncertainties, as determined by the optimisation method of Renne et al. (2011). MSWD: mean square weighted deviation (reduced chi-squared statistic). J: Neutron flux parameter.

	Siletz river volcanic formation				Crescent formation				
Sample	73	103	116	162	389	390	407	441	450
Material	Plagioclase	Plagioclase	Groundmass	Plagioclase	Plagioclase	Plagioclase	Plagioclase	Plagioclase	Plagioclase
J	0.0013955	0.0013895	0.0013977	0.0013931	0.0014038	0.0013865	0.0014054	0.0014054	0.0014052
±J	0.0000070	0.0000069	0.0000070	0.0000070	0.0000070	0.0000069	0.0000070	0.0000070	0.0000070
Inverse variance weighted plateau									
Age (Ma)	48.55	51.48	53.35	58.84	49.49	47.62	58.86	55.96	34.16
± 2s (A)	0.28	0.51	0.24	5.18	0.40	0.28	0.98	0.91	0.39
± 2s (F)	0.29	0.51	0.24	5.21	0.40	0.28	0.99	0.92	0.40
MSWD	1.3	0.11	1.1	1.3	0.68	1.1	0.88	1.3	1.6
N	9	8	7	8	6	10	7	12	10
N-total	17	20	16	14	13	18	18	17	16
%gas	67	82	75	82	85	88	55	85	87
plateau K/Ca	0.019	0.0063	0.035	0.075	0.0114	0.0125	0.0026	0.0030	0.0200
± 2s	0.005	0.0008	0.009	0.013	0.0008	0.0008	0.0003	0.0004	0.0060
Inverse isochron									
Age (Ma)	48.36	51.63	53.04	62.1	49.46	47.44	58.39	56.46	34.23
± 2s (A)	0.61	1.17	1.10	11.1	0.56	0.42	1.37	1.66	0.52
± 2s (F)	0.61	1.18	1.11	11.1	0.57	0.42	1.38	1.67	0.52
n	9	8	7	8	6	10	7	12	10
MSWD	1.4	0.11	1.2	1.4	0.8	1.0	0.9	1.3	1.4
$^{40}Ar/\ ^{36}Ar_{(i)}$	301	293	307	291	296.1	302	302	291	300
±2s	15	18	40	16	8.2	12	14	14	7
Integrated (total fusion)									
Age (Ma)	49.9	52.1	53.9	124.1	55.2	48.7	45.3	62.4	39.9
± 2s (A)	0.2	0.6	0.2	5.3	0.6	0.3	0.7	0.8	0.6
± 2s (F)	0.2	0.6	0.2	5.4	0.6	0.3	0.7	0.8	0.6
$^{40}Ar^{*}/\ ^{39}Ar_{K}$	19.85	20.84	21.43	50.50	21.85	19.50	17.89	24.74	15.73
± 2s	0.09	0.22	0.10	2.27	0.23	0.12	0.29	0.33	0.24

software that can be used to investigate the crystallisation of magmatic systems (Gualda & Ghiorso, 2015). By utilising a database of thousands of experimentally-derived compositions of silicate liquids, MELTS-Excel can calculate the crystallisation sequence, proportions of solid and liquid phases in equilibrium assemblages within a silicate magma. MELTS_Excel can be applied to both hydrous and anhydrous magma compositions over a range of temperature and pressure of 500–2000 °C and <2 GPa respectively, using a number of different redox buffers.

Average major element primary magma compositions were calculated for the Grays River Volcanics, Siletz River, Crescent Formation Group 1 and Group 2 and the Metchosin Igneous Complex by taking the average of the individual primary magmas calculated by PRIMELT3 for each suite or grouping. Each average primary magma was modelled by MELTS_Excel using five scenarios: Model 1, fractional crystallization at 1 kbar (anhydrous); Model 2, fractional crystallization at 1 kbar (1% H_2O); Model 3, fractional crystallisation at 1 kbar (0.25% H_2O); Model 4, fractional crystallization at 3 kbar (anhydrous); Model 5, fractional crystallization at 7 kbar (anhydrous). All models use a quartz–fayalite–magnetite (QFM) oxygen buffer and calculate the composition of the evolving silicate liquid at 5% crystallization intervals until 90% crystallisation of the primary magma. Representative bivariate diagrams showing the liquid lines of descent for each model alongside compositional data for each suite are shown in Fig. 8. Complete model outputs are recorded in Appendix 3.

The majority of the models consistently show that the major element geochemical trends of the constituent suites of Siletzia are best replicated by low pressure (~1 kbar) fractionation occurring in the presence of a small amount (0.25–1 wt. %) of H_2O. These models predict that olivine is the first mineral to crystallise, followed by clinopyroxene and either plagioclase ± spinel, and then by apatite. Inspection of Fig. 8 shows that the majority of the major element variation of the Siletzia suites can be explained by ≤ 70% crystallisation of the primary magma of each suite.

In general, the trace element trends of the Siletzia suite show decreases in the concentrations of compatible trace elements during basaltic fractionation with decreasing MgO with concomitant increases in concentration of the incompatible trace elements (Fig. 4). However, these trends are diffuse as are the trends on incompatible trace elements vs. Zr diagrams (Fig. 5) and so are unlikely to be the product of a single fractionation process. Further, the suites display a range of trace element ratios (Fig. 6) with some samples displaying negative Nb anomalies on primitive-mantle normalised trace element diagrams (e.g., Fig 7F) which are often associated with contamination of a fractionating magma by continental crustal materials (e.g., Nelson et al., 1990; Ciborowski et al., 2014).

Trace elements can be used to test whether the crystallisation of the primary magmas of the suites operated under a purely fractional crystallisation (FC) or assimilation-fractional crystallisation (AFC). To do this, the model that best predicts the major element geochemistry for each Siletzia suite is further tested using trace elements with the equations for Rayleigh fractional crystallisation (Eq. 1) and assimilation-fractional crystallisation (Eq. 2). Representative bivariate diagrams showing the liquid lines of descent for each model alongside compositional data for each suite are shown in Fig. 9. Complete model outputs are recorded in Appendix 3, with preferred modelled parameters for each suite summarised in Table 6.

$$C_l = C_0\left(\left(F^{-(r-1+D)/(r-1)}\right) + \left(\frac{r}{r-1+D}\right)\times\left(\frac{C_A}{C_0}\right)\left(1-\left(F^{-(r-1+D)/(r-1)}\right)\right)\right) \quad (2)$$

Where C_0, C_l and C_A are the concentrations of an element in the primary magma, daughter magma and crustal contaminant (Felsic Crust of Rudnick & Fountain, 1995) respectively. D is the bulk distribution coefficient for the trace element, themselves calculated from the mineral/melt partition coefficients from Bédard (2001). F is the fraction of melt remaining after crystallisation. r is ratio of assimilation rate to the

Table 3
Primary magma major element compositions (wt. %) and thermobarometric results obtained for Siletzia primary magmas studied here, as calculated by PRIMELT3 and FractionatePT†. Olivine addition = the amount of olivine added to the evolved composition in order to produce a primary magma capable of forming through batch melting of fertile peridodite; T_p = mantle potential temperature; F = Degree of melting required to produce a primary magma capable of fractionating olivine in order to produce the evolved composition; Melting pressure = the pressure at which melting occurred at; Melt Model – which melt model (Batch or AFM or both) yielded successful solutions with PRIMELT3.

Sample	SiO_2	TiO_2	Al_2O_3	Cr_2O_3	Fe_2O_3	FeO	MnO	MgO	CaO	Na_2O	K_2O	NiO	P_2O_5	Ol addition (%)	Melt Model	F (%)	Tp (°C)	Tp (°C)†	P melting (Gpa) †
Crescent formation																			
3	45.59	0.83	8.24	-	0.80	10.97	0.17	24.78	7.00	1.45	0.09	-	0.09	54.98	Batch	28	1682	1750	6.40
B019	47.05	1.01	10.47	0.05	0.80	9.42	0.10	18.77	10.46	1.54	0.08	0.16	0.12	32.73	Batch	24	1532	1552	2.89
CM-270	45.79	1.22	9.90	0.02	0.82	10.23	0.24	21.74	8.33	1.34	0.04	0.23	0.10	41.96	Batch	27	1607	1650	4.39
CM-430	45.73	1.11	8.91	0.03	0.80	10.50	0.17	23.10	8.02	1.20	0.10	0.21	0.12	48.54	Batch	29	1641	1694	5.10
CS-404	45.44	1.23	8.52	0.03	0.80	10.80	0.18	23.99	7.27	1.31	0.10	0.21	0.13	52.31	Batch	29	1663	1725	5.82
CS-409	45.27	1.28	8.18	0.03	0.79	10.88	0.17	24.48	7.05	1.23	0.09	0.44	0.12	55.62	Batch	29	1675	1743	6.18
CS-443	45.31	0.72	8.93	0.02	0.82	11.14	0.17	23.81	7.40	1.43	0.02	0.18	0.05	52.63	Batch	25	1658	1725	5.88
DL17	45.23	1.08	10.24	0.02	0.87	10.62	0.21	22.39	7.81	1.19	0.15	0.14	0.07	42.57	Batch	25	1623	1676	4.93
DLs01	45.90	0.92	9.24	0.02	0.80	10.63	0.19	22.53	7.67	1.64	0.21	0.17	0.08	47.58	Batch	25	1627	1675	4.92
DU38	45.97	1.22	11.45	0.03	0.86	9.89	0.22	19.33	9.00	1.66	0.15	0.11	0.12	32.75	Batch	20	1546	1575	3.45
SM91-174	45.63	1.31	9.53	0.03	0.82	10.49	0.18	22.42	7.69	1.44	0.17	0.16	0.12	44.96	Batch	26	1624	1672	4.85
32i	46.97	1.85	11.48	0.01	0.78	9.27	0.20	17.99	9.33	1.83	0.29	-	-	31.19	Batch/AFM	22	1512	1524	2.79
CM-306	46.19	1.27	11.93	0.03	0.89	9.97	0.22	18.01	9.38	1.74	0.15	0.09	0.12	28.52	AFM	19	1513	1535	2.95
CM-316	45.83	1.08	11.96	0.04	0.88	9.75	0.19	19.18	9.58	1.25	0.03	0.14	0.09	30.06	Batch/AFM	21	1543	1571	3.28
DL04c	46.97	0.85	11.18	0.04	0.80	9.49	0.18	18.96	9.30	1.96	0.09	0.12	0.07	33.14	Batch/AFM	24	1537	1555	3.09
DL04r	46.37	0.82	11.30	0.04	0.88	9.81	0.19	19.49	9.18	1.71	0.08	0.07	0.07	30.74	Batch/AFM	22	1551	1577	3.39
Grays river volcanics																			
GR09-10	45.49	2.06	8.44	-	0.96	10.86	0.14	20.83	8.88	1.49	0.59	-	0.27	34.42	Batch	16	1584	1634	4.38
Metchosin igneous complex																			
MET-205	45.93	1.70	9.91	0.04	0.84	10.54	0.18	20.27	8.60	1.41	0.13	0.26	0.20	40.06	AFM	28	1570	1606	3.70
ST-42	45.89	0.68	9.00	0.02	0.76	10.62	0.19	23.94	7.06	1.52	0.06	0.19	0.06	53.51	Batch	30	1662	1716	5.59
ST-43	44.93	0.61	8.22	0.03	0.84	11.56	0.18	24.51	7.29	1.48	0.06	0.25	0.06	55.97	Batch	20	1675	1758	6.78
MIC99-8	46.31	0.77	10.86	0.04	0.84	9.98	0.18	20.05	9.03	1.71	0.01	0.17	0.05	35.37	Batch	23	1565	1595	3.60
MIC99-9	45.97	0.73	9.88	0.04	0.79	10.28	0.15	21.99	8.55	1.31	0.01	0.24	0.06	44.85	Batch	27	1613	1657	4.43
MIC99-13	45.70	0.75	8.22	0.02	0.77	10.72	0.16	25.08	7.21	1.11	0.03	0.18	0.06	56.13	Batch	33	1689	1756	6.33
ME23	46.03	0.74	9.08	0.02	0.82	10.70	0.20	22.31	8.04	1.72	0.14	0.13	0.06	45.99	Batch	24	1621	1670	4.80
ME18	45.82	0.58	9.49	0.03	0.83	10.64	0.19	23.12	7.53	1.52	0.06	0.13	0.06	47.13	Batch	28	1641	1693	5.18
Siletz river formation																			
TM-170	45.62	1.59	9.30	0.03	0.78	10.34	0.18	22.14	8.07	1.32	0.13	0.31	0.18	46.58	Batch	27	1617	1665	4.65
1	46.39	1.23	10.56	-	0.84	9.78	0.18	20.02	9.31	1.50	0.07	-	0.11	33.94	Batch/AFM	25	1564	1593	3.52
372113	45.48	1.14	10.84	0.02	0.92	10.81	0.21	20.70	8.27	1.26	0.16	0.12	0.07	36.69	AFM	26	1581	1622	4.02

Table 4
Major and trace element geochemical data for the samples analysed here which yielded successful solutions with PRIMELT3. Data sources: a – this study, b – Glassley (1974); c – Babcock et al., (1992); d – Moothart (1993); e – Chan et al., (2012); f – Timpa et al., (2005), g – Rarey (1985) and h – Yorath et al., (1999). Full data available in electronic appendix.

	Major elements (wt. %)										Trace elements (ppm)									
	SiO_2	TiO_2	Al_2O_3	$FeO_{(T)}$	MnO	MgO	CaO	Na_2O	K_2O	P_2O_5	Ni	Cr	Zr	Y	Nb	Th	La	Gd	Yb	Source
Crescent Formation																				
3	49.20	1.40	14.10	12.38	0.19	7.70	11.90	2.50	0.16	0.15	-	107	-	-	-	-	2.60	4.69	4.30	b
32i	49.30	2.50	15.60	9.60	0.20	7.10	12.60	2.50	0.40	0.00	-	-	-	-	-	-	-	-	-	b
B019	48.11	1.34	14.02	9.62	0.10	7.39	13.93	2.06	0.10	0.16	111	363	78.36	19.96	6.31	0.55	6.40	3.37	1.85	a
CM-270	47.44	1.78	14.61	10.99	0.25	8.03	12.21	1.99	0.06	0.16	143	157	82.24	27.41	5.30	0.66	8.36	4.34	2.61	a
CM-306	48.30	0.71	17.02	9.06	0.17	7.92	12.43	1.98	0.02	0.30	81	336	36.90	18.81	1.60	0.12	1.53	2.21	2.03	a
CM-316	45.82	1.38	15.45	10.21	0.19	8.75	12.32	1.62	0.04	0.12	157	306	76.99	22.25	9.59	0.50	7.12	3.61	2.10	a
CM-430	47.77	1.73	13.99	11.32	0.18	7.55	12.51	1.89	0.15	0.19	101	272	97.24	28.93	10.67	0.60	8.74	4.40	2.49	a
CS-404	48.06	2.00	13.99	11.93	0.19	7.58	11.86	2.17	0.17	0.21	92	282	116.60	28.87	11.03	0.67	9.75	4.65	2.42	a
CS-409	48.54	2.17	14.00	12.20	0.18	7.44	11.98	2.12	0.15	0.21	179	279	125.91	29.92	13.41	0.91	11.94	5.19	2.61	a
CS-443	46.91	1.15	14.41	11.99	0.18	7.19	11.87	2.33	0.04	0.08	74	166	78.31	30.94	5.28	0.34	3.17	3.87	3.29	a
DL04c	48.45	1.15	15.16	9.81	0.18	7.51	12.54	2.66	0.12	0.09	83	317	71.00	24.00	5.50	2.00	0.00	-	-	c
DL04r	47.68	1.09	15.04	10.53	0.19	9.05	12.17	2.28	0.11	0.09	82	306	69.00	26.00	5.70	1.00	4.00	-	-	c
DL17	46.49	1.58	15.14	11.61	0.22	8.61	11.49	1.77	0.22	0.10	102	152	74.00	25.00	9.50	3.00	0.00	-	-	c
DLs01	48.34	1.43	14.47	11.40	0.20	7.21	11.93	2.59	0.33	0.12	75	165	96.00	34.00	6.40	1.00	12.00	-	-	c
DU38	47.37	1.65	15.56	10.50	0.22	8.21	12.17	2.27	0.20	0.16	95	270	99.00	24.00	12.00	1.00	10.00	-	-	c
SM91 - 174	48.19	2.00	14.70	11.51	0.19	7.97	11.79	2.24	0.26	0.19	88	287	129.00	32.00	12.50	1.00	11.00	-	-	d
Grays river volcanics																				
GR09-10	46.96	2.83	11.69	11.99	0.15	9.53	12.24	2.08	0.82	0.37	-	-	208.00	27.00	34.15	2.82	27.94	7.28	2.04	e
Metchosin igneous complex																				
MET-205	46.90	0.94	16.92	10.27	0.21	7.94	12.60	1.44	0.04	0.09	171	250	51.20	23.18	2.42	0.13	2.87	2.91	2.29	a
MIC99-13	49.59	1.28	14.25	12.18	0.18	7.84	12.42	1.94	0.05	0.10	77	148	98.30	27.20	7.60	-	3.43	4.12	2.91	f
MIC99-8	48.80	1.08	15.38	10.80	0.19	8.34	12.73	2.43	0.02	0.07	139	345	49.50	20.10	5.10	-	2.20	3.02	2.25	f
MIC99-9	49.12	1.12	15.36	11.17	0.16	7.55	13.21	2.04	0.02	0.09	119	346	72.70	24.50	5.20	-	3.35	3.63	2.79	f
ST-42	49.73	1.14	15.21	11.72	0.21	7.17	11.85	2.59	0.10	0.10	68	154	83.00	24.60	4.70	-	2.79	3.75	2.83	f
ST-43	48.35	1.04	14.23	13.15	0.20	7.50	12.53	2.58	0.10	0.10	102	259	71.70	21.90	5.20	-	3.23	3.27	2.46	f
ME23	49.10	1.15	14.20	11.66	0.21	7.57	12.50	2.71	0.22	0.10	76	280	44.00	21.00	-	-	2.60	3.10	-	h
ME18	49.10	0.92	15.10	11.90	0.21	8.24	11.90	2.44	0.09	0.09	64	170	58.00	26.00	-	-	5.30	4.00	-	h
Siletz river formation																				
1	48.60	1.70	14.70	10.57	0.19	8.60	12.90	2.10	0.10	0.16	-	-	-	-	-	-	-	-	-	g
372113	49.19	1.92	10.07	10.56	0.17	13.81	11.49	1.64	0.42	0.23	-	-	-	-	-	-	-	-	-	g
TM-170	47.28	2.42	14.26	10.89	0.18	7.00	12.29	2.03	0.19	0.28	130	301	160.97	26.85	27.63	1.63	20.26	5.56	2.11	a

Table 5
Calculated trace element compositions (ppm) of the Siletzia primary magmas. Calculations completed using equation 1.

Sample	Th	Nb	La	Ce	Pr	Nd	Zr	Hf	Sm	Eu	Ti	Gd	Tb	Dy	Y	Ho	Er	Tm	Yb	Lu
Crescent formation																				
3	-	-	1.17	-	-	8.21	-	-	1.56	0.59	4113	2.16	-	-	-	-	-	-	2.01	0.38
32i	-	-	-	-	-	-	-	-	-	-	10162	-	-	-	-	-	-	-	-	-
B019	0.32	3.67	3.72	8.95	1.17	5.39	45.98	1.23	1.52	0.59	4716	1.99	0.31	1.95	11.79	0.41	1.20	0.18	1.10	0.18
CM-270	0.34	2.73	4.31	10.69	1.60	7.24	42.88	1.23	2.14	0.74	5565	2.28	0.39	2.51	14.42	0.48	1.39	0.21	1.39	0.21
CM-306	0.06	0.76	0.73	1.82	0.33	1.78	17.86	0.50	0.71	0.30	2059	1.08	0.22	1.47	9.19	0.30	0.94	0.15	1.01	0.16
CM-316	0.23	4.26	3.17	7.40	1.10	5.16	34.73	0.93	1.44	0.53	3732	1.64	0.28	1.81	10.14	0.35	0.96	0.16	0.97	0.14
CM-430	0.28	5.06	4.15	10.18	1.52	7.11	46.75	1.30	1.97	0.68	4985	2.13	0.36	2.27	14.04	0.44	1.19	0.19	1.22	0.17
CS-404	0.39	6.34	5.61	13.64	2.06	9.56	67.71	1.60	2.58	0.89	6966	2.71	0.45	2.81	16.88	0.53	1.42	0.22	1.43	0.20
CS-409	0.48	7.04	6.27	15.20	2.27	9.71	66.86	1.83	2.69	0.89	6908	2.78	0.45	2.80	16.02	0.52	1.47	0.21	1.42	0.23
CS-443	0.23	3.55	2.13	6.48	1.03	5.06	53.08	1.43	1.94	0.73	4681	2.64	0.52	3.36	21.08	0.70	2.11	0.35	2.26	0.34
DL04c	1.11	3.03	-	11.03	-	-	39.55	-	-	-	3840	-	-	-	13.47	-	-	-	-	-
DL04r	0.69	3.93	2.76	22.74	-	-	47.84	-	-	-	4530	-	-	-	18.11	-	-	-	-	-
DL17	2.15	6.79	-	12.88	-	-	53.25	-	-	-	6816	-	-	-	18.07	-	-	-	-	-
DLs01	0.70	4.48	8.40	10.51	-	-	67.62	-	-	-	6039	-	-	-	24.06	-	-	-	-	-
DU38	0.67	8.03	6.69	19.42	-	-	66.72	-	-	-	6667	-	-	-	16.26	-	-	-	-	-
SM91 - 174	0.70	8.66	7.63	13.18	-	-	90.01	-	-	-	8370	-	-	-	22.43	-	-	-	-	-
Grays river volcanics																				
GR09-06	0.90	7.76	9.44	21.45	2.90	12.64	94.58	2.31	3.09	1.10	6383	3.31	0.53	3.24	15.30	0.64	1.61	0.23	1.40	0.21
Metchosin igneous complex																				
MET-205	0.08	1.45	1.72	3.76	0.63	3.66	31.01	0.87	1.37	0.54	3417	1.77	0.32	2.26	14.13	0.46	1.39	0.23	1.41	0.21
ST-42	-	2.19	1.30	3.75	0.65	3.42	39.18	1.14	1.17	0.46	3226	1.78	0.33	2.06	11.73	0.46	1.39	0.21	1.37	0.21
ST-43	-	2.29	1.43	3.87	0.60	3.00	32.09	0.85	0.95	0.35	2791	1.48	0.26	1.77	9.91	0.37	1.16	0.19	1.13	0.15
MIC99-8	-	3.30	1.42	4.25	0.73	3.96	32.27	1.09	1.36	0.53	4221	1.98	0.37	2.43	13.18	0.53	1.54	0.22	1.49	0.22
MIC99-9	-	2.87	1.85	4.95	0.84	4.14	40.58	1.14	1.42	0.47	3747	2.04	0.37	2.49	13.78	0.54	1.71	0.29	1.59	0.23
MIC99-13	-	3.34	1.51	4.29	0.70	3.58	43.84	1.04	1.22	0.47	3422	1.85	0.33	2.17	12.26	0.47	1.40	0.20	1.33	0.21
ME23	-	-	1.41	3.57	-	4.18	24.06		0.87	0.38	3016	1.71		2.26	11.58	-	-	-	1.45	-
ME18	-	-	2.81	7.42	-	5.32	31.06		1.50	0.59	3691	2.16		2.65	14.04	-	-	-	1.58	-
Siletz river volcanic formation																				
1	-	-	-	-	-	-	-	-	-	-	5513	-	-	-	-	-	-	-	-	-
TM-170	1.08	18.27	13.40	28.89	3.99	16.95	107.23	2.48	3.81	1.25	9664	3.72	0.58	3.31	17.98	0.59	1.53	0.23	1.42	0.20
372113	-	-	-	-	-	-	-	-	-	-	7354	-	-	-	-	-	-	-	-	-

Table 6
Summary of the modelling of fractional crystallisation of each of the constituent suites of Siletzia. The table indicates the model parameters which best fit the data for each suite.

	MgO (wt. %)	Pressure (kbar)	H_2O (wt%)	Liquidus (°C)	Crystallisation sequence	Preferred mechanism
Crescent Formation						
Group 1	21.88	1	0.25	1480	ol, cpx, plg, sp, opx	FC >> AFC
Group 2	22.20	1	0.25	1485	ol, cpx, plg, sp, opx	FC >> AFC
Siletz River Volcanic Formation	20.95	1	0.25	1465	ol, cpx, sp, plg, opx, ap	-
Metchosin Igneous Complex	22.64	1	1	1475	ol, cpx, sp, plg, opx	FC
Grays River Volcanics	20.83	1	1	1445	ol, cpx, sp, plg, opx, ap	FC

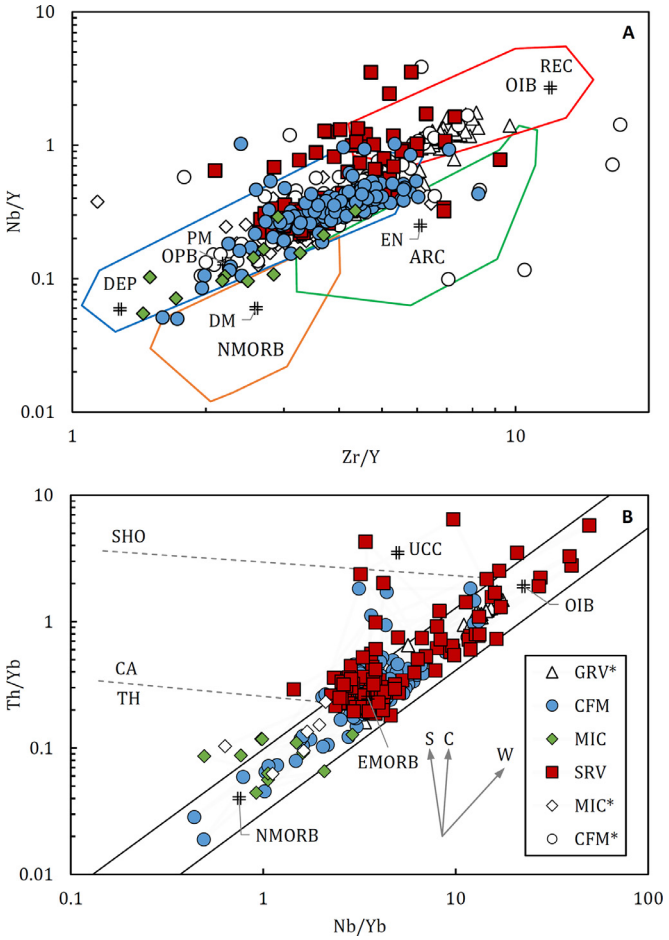

Fig. 6. Bivariate diagrams for: A – Nb/Y vs Zr/Y diagram. Field boundaries and end-member compositions from Condie (2005). PM – primitive mantle, DM – shallow depleted mantle, ARC – arc-related basalts, NMORB – normal mid-ocean ridge basalts, OPB – oceanic plateau basalt, OIB – ocean island basalt, DEP – deep depleted mantle, REC – recycled component; and B – Nb/Yb vs. Th/Yb modified after Pearce (2008) and Manikyamba and Kerrich (2012). The mantle array extends from N-MORB to OIB. TH – tholeiitic; CA – calc-alkaline; SHO – shoshonitic; UCC – upper continental crust. Vectors S, C, and W are vectors for subduction components, crustal contamination, and within-plate evolution respectively. White symbols are literature data. Coloured symbols are new data.

fractional crystallisation rate (taken to be 0.2 in this case based on approaches used in similar magmatic systems (e.g., Gunther et al., 2018; Hari et al., 2018).

The consistent $(Th/Nb)_N$ vs Zr_N observed within the Grays River Volcanics samples indicates that the primary magma of the Grays River Volcanics fractionated without being contaminated by crustal material to any significant degree. Similarly, the trace element systematics of the Metchosin Igneous Complex samples show $(La/Yb)_N$ vs. Zr_N trends which are most similar to those predicted by FC models, and thus contamination can be ruled out as a significant factor here also.

Fractional crystallisation models involving the primary magma derived from the Group 1 Crescent Formation samples can explain the trace element variation for most of the Crescent Formation as a whole. However, a relatively small number of Crescent Formation samples fall on diffuse trends between both the compositions of the primary magmas calculated from the Group 1 and Group 2 samples, and felsic crustal compositions. This may indicate that the Crescent Formation primary magmas fractionated in a number of shallow magma chambers, some of which interacted with, and assimilated their host rocks (potentially terrestrially derived sediments that were transported to the marine environment).

The crystallisation history of the Siletz River Formation remains enigmatic. Neither FC or AFC models of the calculated Siletz River Formation primary magma produces trends in trace element space that convincingly fit the data for the formation. Instead, it is possible that the majority of the Siletz River Formation were formed by still-unconstrained primary magmas, the derivatives of which are too evolved for the approach detailed here, or that the Siletz River Formation is a composite formation made up of fundamentally different suites which, as yet, remain unresolved.

6.3. Conditions of melting

6.3.1. Temperature of melting

Published modelling results have shown that the temperature within a mantle plume would be significantly higher (100–350 °C) than the surrounding mantle (see Campbell, 2007 for a review and Coogan et al., 2014). This prediction has been confirmed by seismic investigation from extant plume-driven magmatic provinces (e.g., Nelson & Grand, 2018; Schutt & Humphreys, 2004; Wolfe et al., 1997).

In order to assess whether the temperature of an ancient mantle source region of a suite of lavas was anomalously hot compared to the ambient upper mantle temperature at that time, it is first necessary to calculate the potential temperature (T_P) of their mantle source. This can be achieved through comparison of the MgO contents of the primary magma calculated by PRIMELT3 with experimentally derived MgO contents of partial melts and solid-state adiabatic gradients (Iwamori et al., 1995). Once calculated, this T_p can be compared to estimates of the temperature of the upper mantle through geological time. This approach is used by Hole and Millett (2016) to estimate the mantle thermal anomaly associated with the emplacement of the North Atlantic Igneous Province who show, crucially, that such an approach yield temperature estimates consistent with seismic interpretations of extant mantle systems.

Various temperature models exist that attempt to show how the upper mantle has cooled since the Archean (e.g., Davies, 2009; Herzberg et al., 2010; Richter, 1988). These models suggest that during the emplacement of Siletzia between ~ 39 and 56 Ma, upper mantle temperatures would have ranged between 1305 °C and 1330 °C. Fig. 10A shows the T_P calculated for the Siletzia primary magmas, as well as the ambient temperature of the upper mantle during the lifetime of the province, as calculated by Davies (2009). The PRIMELT3 modelling (Table 3) shows that the largest range of mantle tempera-

tures (1512–1682°C) are recorded by the Crescent Formation primary magmas and that primary magmas of the remaining suites fall within error of this range. Further, the data show that the Siletzia primary magmas are all derived from mantle significantly hotter (>190 °C) than that calculated for the ambient mantle at the time, as is predicted by mantle plume theory (Campbell, 2007), and confirmed by observation of extant plume systems (e.g., Nelson & Grand, 2018; Schutt & Humphreys, 2004; Wolfe et al., 1997). We therefore conclude that the emplacement of Siletzia was driven by a mantle plume. This finding is supported by the interpretations of others who suggest that Siletzia magmatism formed in response to the impingement of a mantle plume beneath the lithosphere during the early-mid Paleogene (Duncan, 1982; Phillips et al., 2017; Wells et al., 2014). Conversely, this finding does not support other hypotheses for the petrogenesis of Siletzia such as its emplacement in a rift-related marginal basin (Brandon, 2014; Wells et al., 1984), or passive upwelling through a slab window during subduction of a mid-ocean ridge (Babcock et al., 1992), neither of which require (though don't preclude) the input of anomalously hot mantle material.

6.3.2. Depth of melting

Major element ratios such as SiO_2/MgO, CaO/Al_2O_3, and Al_2O_3/TiO_2 in a primary magma are sensitive to the conditions of pressure and temperature under which melting occurs. A number of thermobarometers have been developed in order to determine the depth of mantle melting required to form an observed lava composition (e.g., Herzberg, 1995; Herzberg & Zhang, 1996; Walter, 1998). FractionatePT (Lee et al., 2009) is one such thermobarometer which is applicable to melts derived from peridotitic sources and uses the SiO_2–FeO–MgO–CaO–Na_2O–K_2O contents of primary magmas to determine the temperature and pressure conditions required for melting.

Comparison of the temperature estimates from the PRIMELT3 and FractionatePT thermometers (Appendix 4) show that both thermometers give very similar estimates of melting temperature for the Siletzia primary magmas, and are similar, within error for most of the primary magmas calculated during this study. However, there is a systematic difference in the temperatures calculated by the two thermometers, which, in the case of the primary magmas discussed here, never exceeds 5%.

The good agreement between the two thermometers indicates that the estimates of temperature of melting (Fig. 10A) for the Siletzia province, are robust, and that the FractionatePT barometer, which calculates the pressure of melting can be used with confidence.

Fig. 10B shows the melting pressures (calculated by FractionatePT) for the Siletzia Primary magmas during the lifetime of the province. The data show that the largest range of melting pressures (2.8–6.4 GPa) are recorded by the Crescent Formation primary magmas and that primary magmas of the remaining suites fall, within error, of this range. These pressures of melting, along with the temperatures of melting indicate that the melting occurred at depths consistent with the garnet-lherzolite stability field (Fig. 11).

6.4. Mantle source composition

The behaviour of the REE during partial melting has been quantitatively shown to vary systematically with the degree of partial melting and relative abundance of garnet in the peridotite source (e.g., Song et al., 2009). REE trends of the Grays River Volcanics, Siletz River and Group 1 Crescent Formation cluster around trends defined by melts derived from the melting of garnet peridotite. Conversely, the most primitive samples from the Metchosin Igneous Complex and Group 2 Crescent Formation have $(Gd/Yb)_N \approx$ primitive mantle values, which are more indicative of melting occurring within the spinel stability field (Fig. 7).

However, the conditions of melting, as calculated from the Siletzia primary magmas suggest that all of the Siletzia primary magmas were derived from garnet-bearing peridotite (Fig. 11). Typically, magmas derived from the partial melting of garnet-bearing peridotites record trace element compositions characterised, in part, by steeply dipping HREE patterns on primitive mantle-normalised trace element diagrams (e.g., Kushiro, 1996; McKenzie & O'Nions, 1991). Such patterns are observed in the primary magmas of the Siletz River, Grays River Volcanics and Group 1 of the Crescent Formation (Fig. 7). However, the Metchosin Igneous Complex and Group 2 Crescent Formation have flat HREE patterns on primitive mantle-normalised diagrams, more characteristic of melting occurring in the absence of garnet - despite recording similar degrees of partial melting and depths of melting to the other primary magmas discussed (Table 3).

This apparent contradiction between the conditions of partial melting and the calculated trace element geochemistry of the primary magmas can be most easily explained by differences in the modal mineralogy of the mantle source regions from which the primary magmas were derived. Specifically, the primary magmas of the Siletz River, Grays River Volcanics and Group 1 Crescent Formation were likely derived from garnet-bearing peridotite, where garnet was in sufficient abundance to remain in the residue up to the significant degrees of partial melting ($\leq$ 29%) recorded by some of the primary magmas (Table 3). Conversely, the Metchosin Igneous Complex and Group 2 Crescent Formation primary lavas were most likely derived from garnet-bearing peridotite that had sufficiently low abundances of garnet such that the garnet was completely melted during the formation of the primary magmas from these suites (e.g., Walter, 1998).

6.5. Evolution of the Siletz plume

All of the primary magmas calculated by PRIMELT3 for Siletzia are derived from anomalously hot mantle, as is predicted by plume models (Campbell, 2007), and this is the petrogenetic mechanism we favour for the formation of the province. The calculated primary magma trace element compositions (Fig. 7) suggest that the plume sampled a range of mantle reservoirs common to OIBs (e.g., Jackson & Dasgupta, 2008), and potentially a third source (or mixture of sources) with a composition intermediate between that of OIBs and another less incompatible element-enriched reservoir. Therefore, aside from the anomalously high temperature of the Siletzia primary magmas, models invoking a mantle plume origin are further suggested by the identification of an OIB-like mantle (e.g., Condie 2005).

The plume paradigm has been argued for by others as a plausible mechanism to explain the origin of constituent suites of Siletzia. Quite often, such models link the proposed Siletz plume with the mantle plume currently driving magmatism within the Yellowstone Plateau, itself widely argued to be responsible for the volcanism preserved in the Columbia River Basalts and Snake River Plain (Brandon & Goles, 1988; Camp et al., 2015; Geist et al., 2002). Duncan (1982) suggests such a link, partly on the basis on absolute plate motions, and argues that the nascent Yellowstone plume emplaced the Siletz Terrane as an oceanic island chain, proximal to the northwest Pacific coast of ancestral North America. The subsequent accretion of the Siletz Terrane and continuing westward movement of the North American plate over the Yellowstone plume is argued by Duncan (1982) and Murphy et al. (2003) to explain the apparent eastward younging of magmatism associated with the Siletz Terrane, Columbia River Basalt Province and Yellowstone – Snake River Plain. This interpretation is similar to that argued for by Wells et al. (2014), who suggest that the rapid emplacement, and OIB-like compositional characteristics of the Siletz Terrane are indicative of the terrane being derived from a mantle plume.

Comparison of the trace element composition of the most primitive lavas of Siletzia with similarly primitive lavas of the constituent suites of the Yellowstone Magmatic Province (YMP) (Fig. 12A) shows that the highest concentration of analyses from both provinces share an Oceanic Plateau Basalt-like geochemistry. Though the analyses of the YMP span a much broader compositional range than those of Siletzia, the significant overlap in analyses indicate that the two provinces were derived from mantle regions that shared a similar composition.

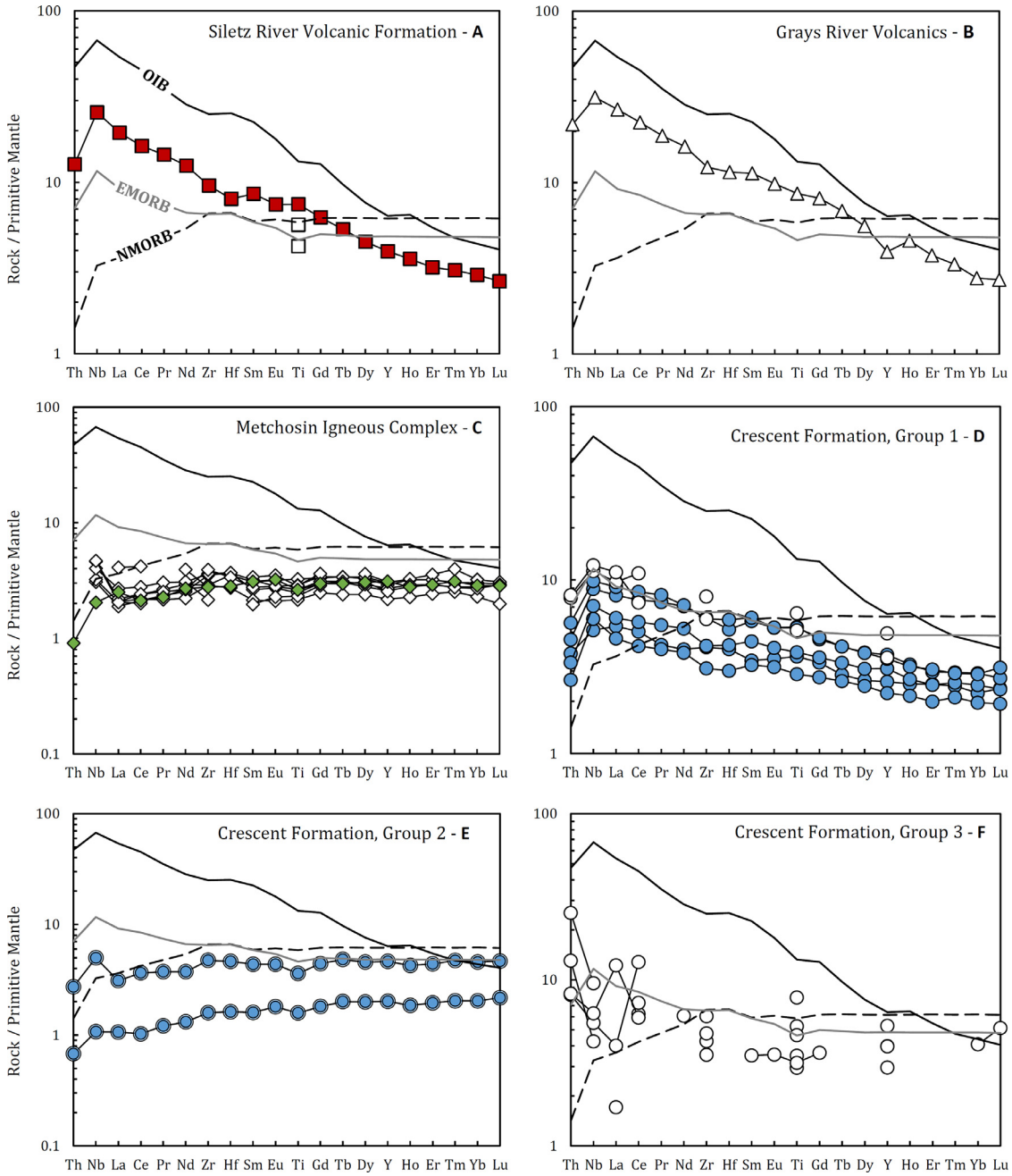

Fig. 7. Primitive mantle-normalised trace element diagrams of the Siletzia primary magmas, estimated by accounting for the effect of the olivine fractionation (Eq. 1) as calculated by PRIMELT3 for each sample (Table 3). Normalisation factors taken from McDonough and Sun (1995). NMORB, EMORB and OIB compositions taken from Sun and McDonough (1989). White symbols are literature data. Coloured symbols are new data.

In terms of isotopes, Pyle et al. (2009) argues that parts of the Siletz Terrane are isotopically indistinguishable from parts of the CRBP and uses this as evidence of a probable cogenetic link between the two, with the Siletz Terrane representing melting of the nascent Yellowstone plume head, and the Columbia River Basalts related to melting of the plume tail. Pyle et al. (2009) and Chan et al. (2012) have used similar arguments to suggest that the Grays River Volcanics were also derived from the Yellowstone plume, which supplied the primary magmas of the suite via a slab window within the partially-subducted Juan de Fuca Plate. However, further isotopic analysis by Phillips et al. (2017), reveals some isotopic differences between the Siletz Terrane and the Columbia River Basalts which are difficult to reconcile with a cogenetic origin for both the Siletz Terrane and CRBP. Instead, Phillips et al. (2017) suggest these compositional differences may be the result of melting of a heterogenous plume head, or alternatively melting of plume(s) unrelated to that which produced the CRBP.

Published isotopic data for Siletzia are shown alongside isotopic data for the YMP in Fig. 12B and 12C. In terms of Nd and Sr isotopic space (Fig. 12B), the Siletzia lavas cluster around HIMU and PREMA compositions, with very few Siletzia samples trending toward more enriched compositions. The samples from YMP define an expansive trend from PREMA compositions towards EM2. Interestingly, several of the oldest YMP samples (from the Columbia River Basalt Province) overlap with the Siletzia cluster, while the youngest YMP samples (from the Yellowstone Plateau) fall entirely outside of the Siletzia cluster and plot in more enriched isotope space. In terms of Pb isotopes (Fig. 12C), a sim-

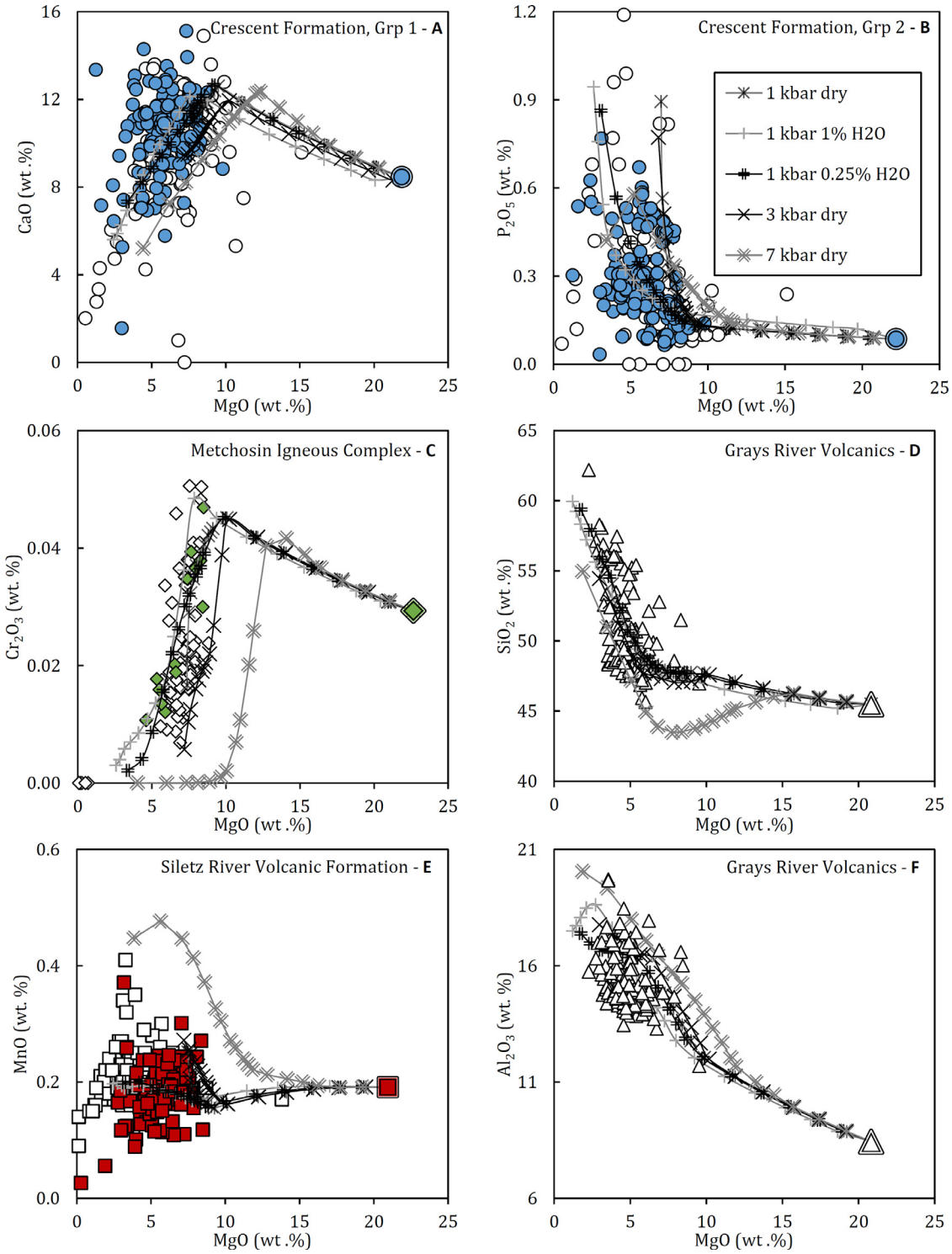

Fig. 8. Representative major element vs. MgO bivariate diagrams of the Siletzia samples, alongside the average major element composition of each primary magma (larger, compound border symbol). Also shown are the liquid lines of descent predicted by Melts_EXCEL for each primary magmas under the model paramters described in the text. Markers on models indicate increments of 5% crystallisation. Note that major element chemistry of each suite is best approximated by low pressure crystallisation (1 kbar) with 0.25–1 wt % H_2O. Complete model outputs available in the electronic appendix. White symbols are literature data. Coloured symbols are new data.

ilar pattern is seen, whereby the Siletzia samples define a tight trend between PREMA and HIMU compositions with a small number of samples trending towards EM2 compositions. In this space, the YMP samples from the Columbia River Basalt Province show partial overlap with the Siletzia grouping, while the youngest YMP samples from the Yellowstone Plateau plot away from the Siletzia grouping closest towards EM1 compositions.

Therefore, although some trace element compositional similarity exists between the lavas of the two provinces, the wide range of compositions within the YMP makes any such comparison equivocal and cannot,

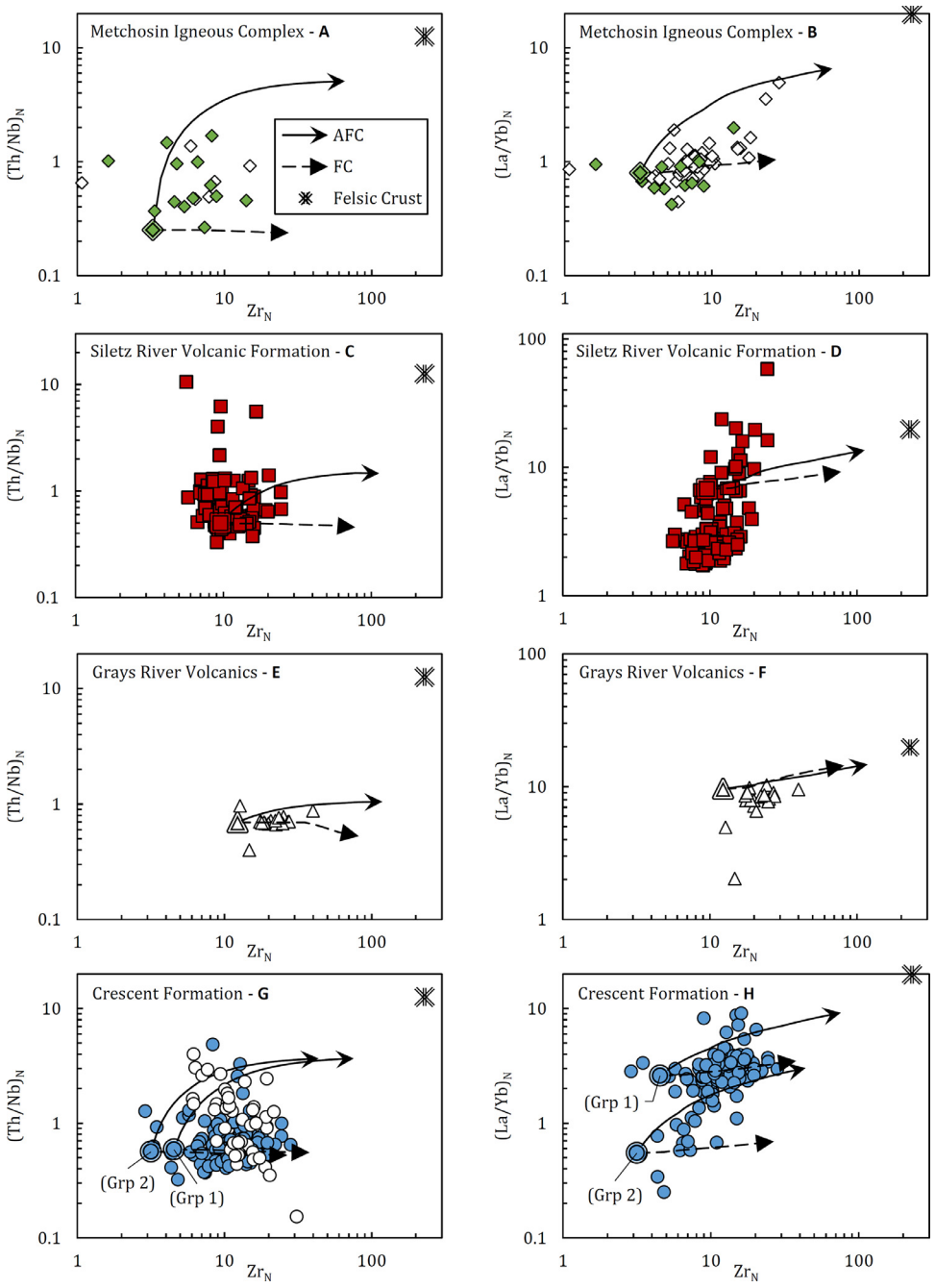

Fig. 9. Primitive mantle-normalised bivariate diagrams showing the trace element evolution of the Siletzia primary magmas (double outline) via modelled FC (dashed line) and AFC (solid line) pathways. AFC models contamination using the Felsic Crust composition of Rudnick and Fountain (1995) and an r value of 0.2. White symbols are literature data. Coloured symbols are new data.

alone, be used to argue for a cogenetic origin. Examination of the YMP and Siletzia isotopic systems better delineate potential mantle sources than trace elements do. These isotopes show that the oldest parts of the YMP share an isotopic composition, similar to (the relatively homogenous) Siletzia. This similarity disappears with the youngest YMP samples, and we interpret this to potentially show a secular change in mantle source region sampled by the Yellowstone Plume over time.

6.6. Environmental impact

The formation of LIPs has been shown to have significant impacts on the atmosphere, biosphere and hydrosphere and have been correlated to many first and second order extinction events (e.g., Bond et al., 2014; Kerr, 2005). The Palaeocene-Eocene Thermal Maximum (PETM) represents an abrupt climate warming of 5–8 °C at around 55.5 Ma (McInerney & Wing, 2011; Westerhold et al., 2012). and is marked by a global temperature rise inferred from a >1 ‰ negative excursion in $\delta^{18}O$ of benthic foraminifera, indicating around a 5 °C increase in the temperature of deep waters (Zachos et al., 2001).

The PETM is thought to be the result of a catastrophic release of several thousands of petagrams (Pg) of carbon into the ocean-atmosphere system (Dickens et al., 1997), which is inferred from the large global negative carbon isotopic excursion and the extensive dissolution of deep-ocean carbonates (McInerney & Wing, 2011). The PETM itself was a relatively short lived event that lasted around 200 ka (McInerney & Wing, 2011), with the carbon release spanning less than 20 ka (but it may have occurred in less than a year according to some estimates (Bowen et al., 2015; Higgins & Schrag, 2006). With the exception of benthic foraminifera, relatively few groups suffered major extinctions despite most terrestrial and marine organisms experiencing large shifts in geographic distribution, rapid evolution and changes in trophic ecol-

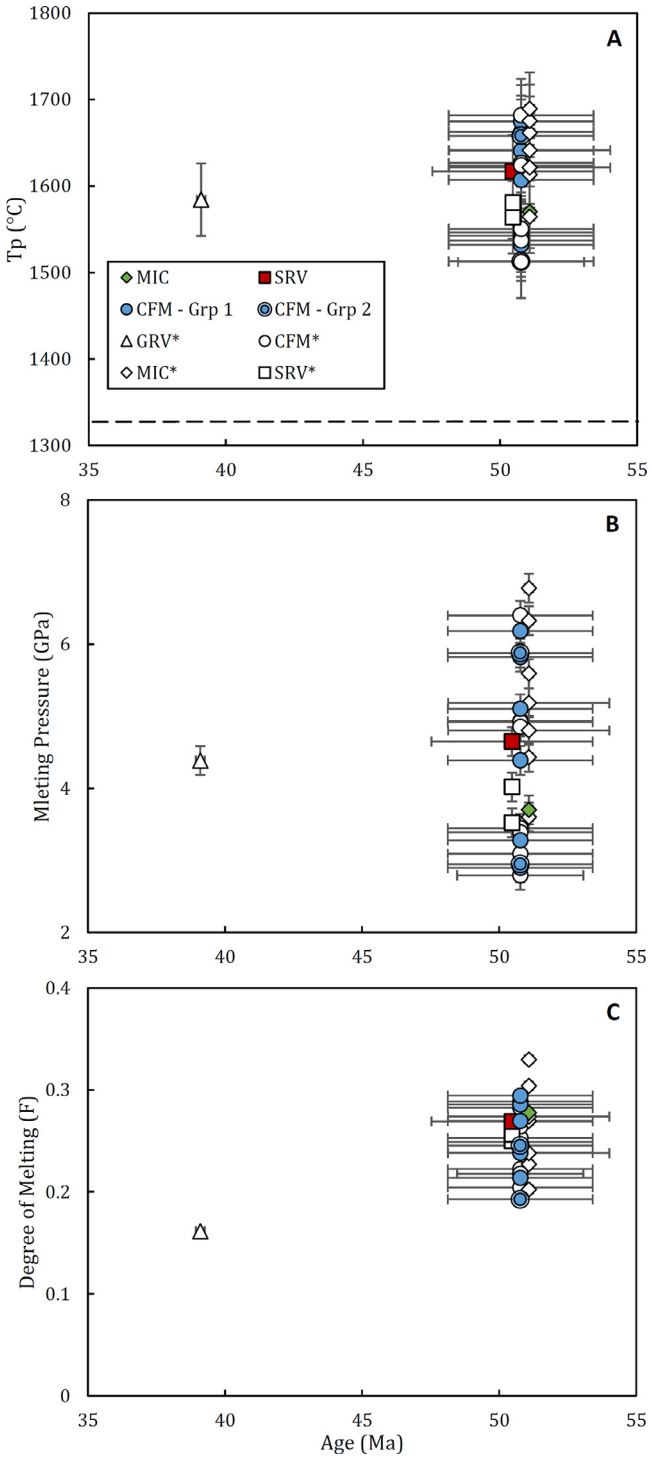

Fig. 10. Thermobarometric results for Siletzia samples successfully computed by PRIMELT3. A – Mantle potential temperature (T_P) as calculated by PRIMELT3. *y*-axis error bars = 42 °C (Herzberg and Asimow, 2015). Also shown (dashed) is the contemporary temperature of the upper mantle using the mantle cooling curve of Davies (2009); B – Melting pressures as calculated by FractionatePT. *y*-axis error bars = 0.2 GPa (Lee et al. 2009); C – Degree of Partial Melting as calculated by PRIMELT3. *x*-axis error bars for MIC and CFM taken from U-Pb age range and midpoint of Eddy et al. (2017). *x*-axis error bars for SRV taken from Ar–Ar age range and midpoint of new data (Table 2). White symbols are literature data. Coloured symbols are new data.

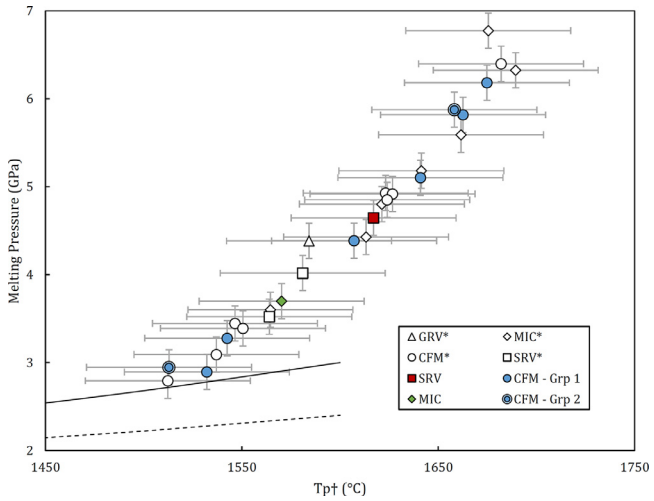

Fig. 11. Diagram showing the pressure and temperature conditions of the transition of spinel lherzolite to garnet lherzolite as estimated by Klemme and O'Neill (2000) - solid line and (Gasparik, 1984) - dashed line. Also shown are the melting pressure (FractionatePT) and temperatures (PRIMELT3) for the Siletzia primary magmas respectively. Error bars as in Fig. 10. White symbols are literature data. Coloured symbols are new data.

ogy (McInerney & Wing, 2011). The age of onset of the PETM has been estimated at around 56 Ma using radiometric dates of marine ash layers and orbital timing of marine sediments (Westerhold et al., 2009), while the upper boundary of the negative carbon isotopic excursion (calculated from zircons in the upper part of the sequence) is thought to be 56.09 ± 0.03 Ma, (Jaramillo et al., 2010).

Estimates for the exact amount of C released into the biosphere during the PETM vary widely from 3000 Pg to ~10,000 Pg (Cui et al., 2011; Zeebe et al., 2009), while recent work (Gutjahr et al., 2017), suggests that the carbon source is isotopically heavy likely to be volcanic in origin. Similarly unconstrained are estimates of the flux of this C into the biosphere over time. Recent modelling (Gutjahr et al., 2017) has suggested that a cumulative release of ~10,000–12,000 Pg of C during the PETM would be required in order to drive the carbon isotope excursion observed in foraminiferal records that span the PETM. Arguing for a role for the North Atlantic Igneous Province (NAIP) in the triggering of the PETM, Gutjahr et al. (2017) multiply the estimated magmatic volumes of the NAIP by the 3600–6000 g/m^3 of C that are typically released by degassing magmas (Saunders, 2015). Gutjahr et al. (2017) argue that the resultant 18,000–60,000 Pg of C released by the NAIP eruptions would have been sufficiently large to drive the C isotope excursion observed in the geological record at the onset of the PETM.

Though the majority of the Ar–Ar dating presented here, and other recent high-precision U–Pb analyses (Eddy et al., 2017), rules Siletzia out as a potential initiating mechanism for the onset of the PETM, its potential effect on global climate warrants further investigation. Comparison of the eruptive ages of Siletzia with temperature records at the time (Fig. 13) show that the eruption ages of the suites of the Siletz Terrane coincide with some of the highest sea-surface temperatures recorded during the Eocene (Evans et al., 2018). Following the same approach as Gutjahr et al. (2017) and applying it to the estimated volume (2.6×10^6 km^3) of the Siletz Terrane (Phillips et al., 2017; Trehu et al., 1994), we estimate that a potential 9360–15,600 Pg of C may have been added to the biosphere during emplacement of the terrane. Even before taking into account any potential positive feedbacks this new C flux might have had on atmospheric CO_2 at the time, we propose that the greenhouse effect of the eruption of Siletzia to have been sufficiently large to have contributed to the ~35 °C sea-surface temperature maxima observed in the Eocene climate record (Evans et al., 2018).

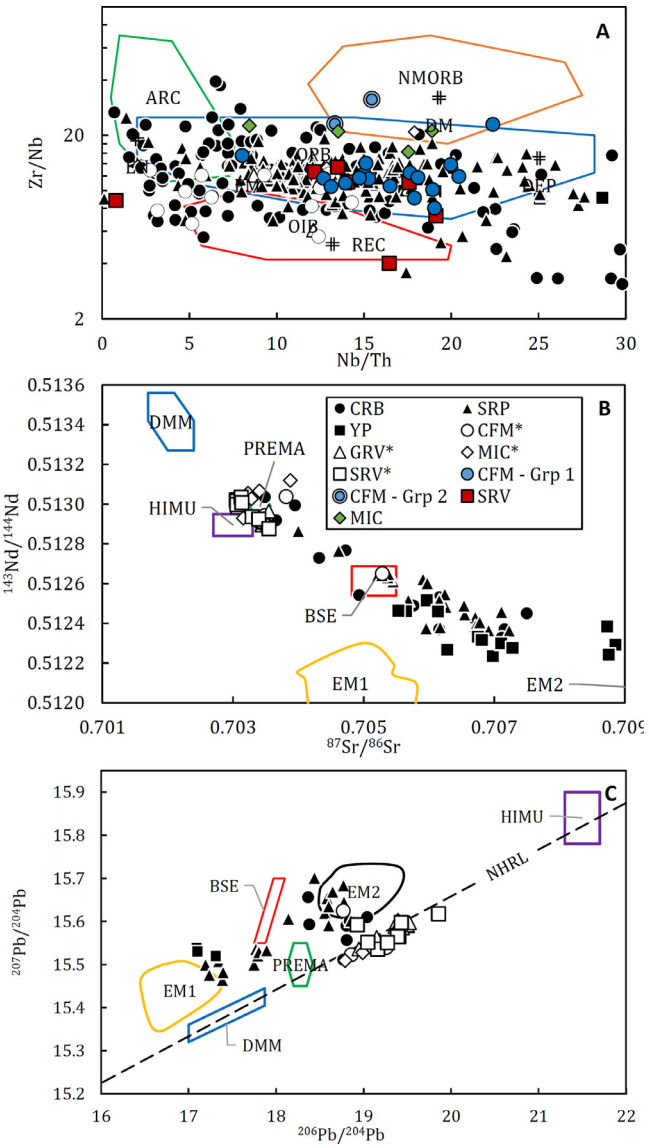

Fig. 12. Bivariate diagrams for: A – Nb/Th vs. Zr/Nb (Condie 2005) showing the > 7.5 wt% MgO samples from Siletzia presented here, along with the > 7.5 wt% MgO Yellowstone Magmatic Province (YMP) which itself is composed of the Columbia River Basalt (CRB), Snake River Plain (SRP) and Yellowstone Plateau (YP); B – $^{87}Sr/^{86}Sr$ vs. $^{143}Nd/^{144}Nd$, and; C – $^{206}Pb/^{204}Pb$ vs. $^{207}Pb/^{204}Pb$, both showing isotopic compositions of >7.5 wt% MgO samples from Siletzia (Phillips et al., 2017) and the YMP, showing the main oceanic mantle reservoirs of Zindler and Hart (1986). White symbols are literature data. Coloured symbols are new data. Data for the YMP extracted from the GeoRoc compilation (http://georoc.mpch-mainz.gwdg.de/).

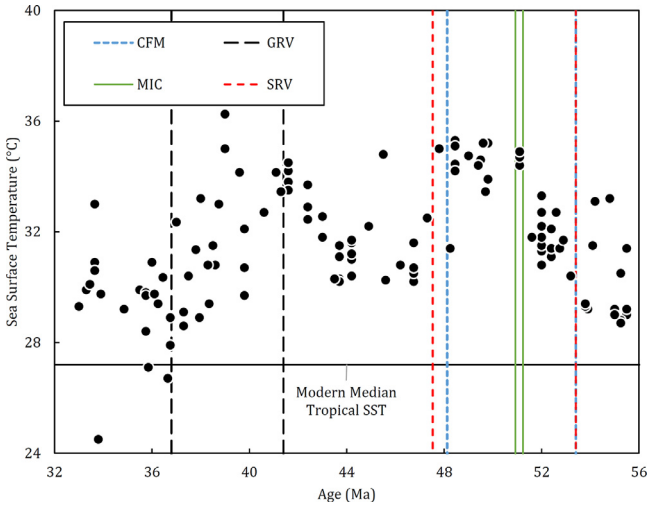

Fig. 13. Evolution of tropical Sea Surface Temperature through the Eocene, taken from Fig. 4 in Evans et al. (2018). Vertical lines indicate ages of Siletzia volcanism using ranges described in Fig. 10.

7. Conclusions

1. The magmatism preserved within Siletzia was driven by the melting of anomalously hot mantle, several hundred degrees hotter than the ambient mantle at the time, and is consistent with a mantle plume model for the petrogenesis of the province.
2. The Siletzia plume sampled a restricted range of mineralogically diverse mantle reservoirs during the lifetime of the province. Some of these source regions are similar in composition to reservoirs which feed modern Ocean Island, and Mid-Ocean Ridge volcanic systems.
3. The primary magmas formed during partial melting of the Siletzia mantle reservoirs were able to rise through the crust until they ponded in shallow (~1 kbar) magma chambers. Here the majority of the magmas evolved through simple fractional crystallisation, with a minority interacting with their crustal host rocks.
4. Isotopic evidence suggests that most of the Siletzia lavas are distinct from most of the Yellowstone Magmatic Province samples. However, there is a compositional overlap between the Siletzia samples and the oldest parts the Yellowstone Magmatic Province. This may indicate a cogenetic link between the provinces, whereby the mantle source sampled by the plume has changed over time.
5. The onset of Siletzia volcanism is broadly coincident with the highest recorded Eocene sea surface temperatures. This timing, along with the magmatic volume of the province, make Siletzia a plausible contributary cause of the biospheric perturbation observed in the geological record at this time, and thus warrants further study.

Declaration of Competing Interest

The authors declare that they have no known competing financial interests or personal relationships that could have appeared to influence the work reported in this paper.

Acknowledgements

The research presented in this paper forms part of a PhD dissertation undertaken by B.A. Phillips at Cardiff University. Iain McDonald is thanked for the major and trace element analyses of the samples. This work was supported by a Natural Environmental Research Council doctoral training grant (grant number NE/L501773/1).

Supplementary materials

Supplementary material associated with this article can be found, in the online version, at doi:10.1016/j.ringeo.2020.100004.

References

Babcock, R. S., Burmester, R., Engebretson, D. C., Warnock, A., & Clark, K. P. (1992). A rifted margin origin for the Crescent basalts and related rocks in the northern coast range volcanic province, Washington and British Columbia. *Journal of Geophysical Research: Solid Earth, 97*, 6799–6821.

Bédard, J. (2001). Parental magmas of the Nain Plutonic suite anorthosites and mafic cumulates: a trace element modelling approach. *Contributions to Mineralogy and Petrology, 141*, 747–771.

Bond, D. P. G., Wignall, P. B., Keller, G., & Kerr, A. C. (2014). *Large igneous provinces and mass extinctions: An update, volcanism, impacts, and mass extinctions: causes and effects* (pp. 29–55). Geological Society of America.

Bowen, G. J., Maibauer, B. J., Kraus, M. J., Röhl, U., Westerhold, T., Steimke, A., Gingerich, P. D., Wing, S. L., & Clyde, W. C. (2015). Two massive, rapid releases of carbon during the onset of the Palaeocene–Eocene thermal maximum. *Nature Geoscience, 8*, 44.

Brandon, A. D., & Goles, G. G. (1988). A Miocene subcontinental plume in the Pacific Northwest: Geochemical evidence. *Earth and Planetary Science Letters, 88*, 273–283.

Brandon, M. T. (2014). New evidence for backarc basin interpretation for Eocene coast-range terrane. In *Proceedings 2014 GSA annual meeting in Vancouver*.

Bryan, S. E., & Ernst, R. E. (2008). Revised definition of Large Igneous Provinces (LIPs). *Earth-Science Reviews, 86*, 175–202.

Bryan, S. E., & Ferrari, L. (2013). Large igneous provinces and silicic large igneous provinces: Progress in our understanding over the last 25 years. *GSA Bulletin, 125*, 1053–1078.

Bukry, D., & Snavely, P. D. (1988). Coccolith zonation for Paleogene strata in the Oregon coast range. In M. Filewicz, & R. Squires (Eds.), *Paleogene stratigraphy, West coast of North America: pacific section, society of economic paleontologists and mineralogists, West coast Paleogene symposium* (pp. 251–263).

Camp, V. E., Pierce, K. L., & Morgan, L. A. (2015). Yellowstone plume trigger for Basin and range extension, and coeval emplacement of the Nevada–Columbia Basin magmatic belt. *Geosphere, 11*, 203–225.

Campbell, I. H. (2007). Testing the plume theory. *Chemical Geology, 241*, 153–176.

Campbell, I. H., & Griffiths, R. W. (1990). Implications of mantle plume structure for the evolution of flood basalts. *Earth and Planetary Science Letters, 99*, 79–93.

Chambers, L. M., Pringle, M. S., & Fitton, J. G. (2004). Phreatomagmatic eruptions on the Ontong Java Plateau. In *Phreatomagmatic eruptions on the Ontong Java Plateau: 229* (pp. 325–331). Geological Society, London, Special Publications.

Chan, C., Tepper, J., & Nelson, B. (2012). Petrology of the Grays river volcanics, southwest Washington: Plume-influenced slab window magmatism in the Cascadia forearc. *Geological Society of America Bulletin, 124*, 1324–1338.

Chen, L., Sun, Y., Pei, X., Gao, M., Feng, T., Zhang, Z., & Chen, W. (2001). Northernmost paleo-tethyan oceanic basin in Tibet: Geochronological evidence from 40 Ar/39 Ar age dating of Dur'ngoi ophiolite. *Chinese Science Bulletin, 46*, 1203–1205.

Ciborowski, T. J. R., Kerr, A. C., McDonald, I., Ernst, R. E., Hughes, H. S. R., & Minifie, M. J. (2014). The geochemistry and petrogenesis of the Paleoproterozoic du Chef dyke swarm, Québec, Canada. *Precambrian Research, 250*, 151–166.

Coffin, M., Pringle, M., Duncan, R. A., Gladczenko, T. P., Storey, M., Müller, D., & Gahagan, L. (2002). Kerguelen hotspot magma output since 130 Ma. *Journal of Petrology, 43*, 1121–1139.

Coffin, M. F., & Eldholm, O. (1994). Large igneous provinces: Crustal structure, dimensions, and external consequences. *Reviews of Geophysics, 32*, 1–36.

Condie, K. C. (2005). High field strength element ratios in Archean basalts: A window to evolving sources of mantle plumes? *Lithos, 79*, 491–504.

Coogan, L. A., Saunders, A. D., & Wilson, R. N. (2014). Aluminum-in-olivine thermometry of primitive basalts: Evidence of an anomalously hot mantle source for large igneous provinces. *Chemical Geology, 368*, 1–10.

Cui, Y., Kump, L. R., Ridgwell, A. J., Charles, A. J., Junium, C. K., Diefendorf, A. F., Freeman, K. H., Urban, N. M., & Harding, I. C. (2011). Slow release of fossil carbon during the Palaeocene–Eocene thermal maximum. *Nature Geoscience, 4*, 481–485.

Davies, G. F. (2009). Effect of plate bending on the Urey ratio and the thermal evolution of the mantle. *Earth and Planetary Science Letters, 287*, 513–518.

Dickens, G. R., Castillo, M. M., & Walker, J. C. (1997). A blast of gas in the latest Paleocene: Simulating first-order effects of massive dissociation of oceanic methane hydrate. *Geology, 25*, 259–262.

Duncan, R. A. (1982). A captured island chain in the Coast range of Oregon and Washington. *Journal of Geophysical Research, 87*, 827.

Duncan, R. A. (2002). A time frame for construction of the Kerguelen plateau and broken ridge. *Journal of Petrology, 43*, 1109–1119.

Eddy, M. P., Clark, K. P., & Polenz, M. (2017). Age and volcanic stratigraphy of the Eocene Siletzia oceanic plateau in Washington and on Vancouver Island. *Lithosphere, 9*, 652–664.

Ernst, R. E., Liikane, D. A., Jowitt, S. M., Buchan, K. L., & Blanchard, J. A. (2019). A new plumbing system framework for mantle plume-related continental large igneous Provinces and their mafic-ultramafic intrusions. *Journal of Volcanology and Geothermal Research, 384*, 75–84.

Ernst, R. E. (2014). *Large igneous provinces*. Cambridge University Press.

Ernst, R. E., & Bleeker, W. (2010). Large igneous provinces (LIPs), giant dyke swarms, and mantle plumes: significance for breakup events within Canada and adjacent regions from 2.5 Ga to the Present. *Canadian Journal of Earth Sciences, 47*, 695–739.

Evans, D., Sagoo, N., Renema, W., Cotton, L. J., Müller, W., Todd, J. A., Saraswati, P. K., Stassen, P., Ziegler, M., Pearson, P. N., Valdes, P. J., & Affek, H. P. (2018). Eocene greenhouse climate revealed by coupled clumped isotope-Mg/Ca thermometry. *Proceedings of the National Academy of Sciences, 115*, 1174–1179.

Fitton, J. G., & Godard, M. (2004). Origin and evolution of magmas on the Ontong java plateau. In *Origin and evolution of magmas on the Ontong java plateau: 229* (pp. 151–178). Geological Society, London, Special Publications.

Gasparik, T. (1984). Two-pyroxene thermobarometry with new experimental data in the system CaO–MgO–Al_2O_3–SiO_2. *Contributions to Mineralogy and Petrology, 87*, 87–97.

Geist, D. J., Sims, E. N., Hughes, S. S., & McCurry, M. (2002). Open-system evolution of a single episode of Snake River Plain magmatism. In P. K. Link, & L. L. Mink (Eds.), *Geology, Hydrogeology, and Environmental Remediation: Idaho National Engineering and Environmental Laboratory, eastern Snake River plain, Idaho* (p. 0). Geological Society of America.

Glassley, W. (1974). Geochemistry and tectonics of the crescent volcanic rocks, Olympic Peninsula, Washington. *Geological Society of America Bulletin, 85*, 785–794.

Gualda, G. A. R., & Ghiorso, M. S. (2015). MELTS_excel: A microsoft excel-based MELTS interface for research and teaching of magma properties and evolution. *Geochemistry, Geophysics, Geosystems, 16*, 315–324.

Günther, T., Haase, K. M., Klemd, R., & Teschner, C. (2018). Mantle sources and magma evolution of the Rooiberg lavas, Bushveld large igneous Province, South Africa. *Contributions to Mineralogy and Petrology, 173*, 51.

Gutjahr, M., Ridgwell, A., Sexton, P. F., Anagnostou, E., Pearson, P. N., Pälike, H., Norris, R. D., Thomas, E., & Foster, G. L. (2017). Very large release of mostly volcanic carbon during the Palaeocene–Eocene thermal maximum. *Nature, 548*, 573.

Haeussler, P. J., Bradley, D. C., Wells, R. E., & Miller, M. L. (2003). Life and death of the Resurrection plate: Evidence for its existence and subduction in the northeastern Pacific in Paleocene–Eocene time. *Geological Society of America Bulletin, 115*, 867–880.

Hari, K. R., Swarnkar, V., & Prasanth, M. M. (2018). Significance of assimilation and fractional crystallization (AFC) process in the generation of basaltic lava flows from Chhotaudepur area, Deccan large igneous province, NW India. *Journal of Earth System Science, 127*, 85.

Hartley, M., & Thordarson, T. (2009). Melt segregations in a Columbia river basalt lava flow: A possible mechanism for the formation of highly evolved mafic magmas. *Lithos, 112*, 434–446.

Hastie, A. R., Fitton, J. G., Kerr, A. C., McDonald, I., Schwindrofska, A., & Hoernle, K. (2016). The composition of mantle plumes and the deep Earth. *Earth and Planetary Science Letters, 444*, 13–25.

Herzberg, C. (1995). Generation of plume magmas through time: An experimental perspective. *Chemical Geology, 126*, 1–16.

Herzberg, C. (2004). Partial melting below the Ontong java plateau. In *Partial melting below the Ontong java plateau: 229* (pp. 179–183). Geological Society, London, Special Publications.

Herzberg, C., & Asimow, P. D. (2008). Petrology of some oceanic island basalts: PRIMELT2.XLS software for primary magma calculation. *Geochemistry, Geophysics, Geosystems, 9*, Q09001.

Herzberg, C., & Asimow, P. D. (2015). PRIMELT3 MEGA.XLSM software for primary magma calculation: Peridotite primary magma MgO contents from the liquidus to the solidus. *Geochemistry, Geophysics, Geosystems, 16*, 563–578.

Herzberg, C., Asimow, P. D., Arndt, N., Niu, Y., Lesher, C., Fitton, J., Cheadle, M., & Saunders, A. (2007). Temperatures in ambient mantle and plumes: Constraints from basalts, picrites, and komatiites. *Geochemistry, Geophysics, Geosystems, 8*, 1–34.

Herzberg, C., Condie, K., & Korenaga, J. (2010). Thermal history of the Earth and its petrological expression. *Earth and Planetary Science Letters, 292*, 79–88.

Herzberg, C., & Zhang, J. (1996). Melting experiments on anhydrous peridotite KLB-1: Compositions of magmas in the upper mantle and transition zone. *Journal of Geophysical Research: Solid Earth, 101*, 8271–8295.

Higgins, J. A., & Schrag, D. P. (2006). Beyond methane: towards a theory for the Paleocene–Eocene thermal maximum. *Earth and Planetary Science Letters, 245*, 523–537.

Hirsch, D. M., & Babcock, R. S. (2009). Spatially heterogeneous burial and high-P/T metamorphism in the Crescent Formation, Olympic Peninsula, Washington. *American Mineralogist, 94*, 1103–1110.

Hole, M. J., & Millett, J. M. (2016). Controls of mantle potential temperature and lithospheric thickness on magmatism in the North Atlantic Igneous Province. *Journal of Petrology, 57*, 417–436.

Ichiyama, Y., Ishiwatari, A., Kimura, J. I., Senda, R., & Miyamoto, T. (2014). Jurassic plume-origin ophiolites in Japan: Accreted fragments of oceanic plateaus. *Contributions to Mineralogy and Petrology, 168*, 1–24.

Irvine, T. N. J., & Baragar, W. R. A. (1971). A guide to the chemical classification of the common volcanic rocks. *Canadian Journal of Earth Sciences, 8*, 523–548.

Iwamori, H., McKenzie, D., & Takahashi, E. (1995). Melt generation by isentropic mantle upwelling. *Earth and Planetary Science Letters, 134*, 253–266.

Jackson, M. G., & Dasgupta, R. (2008). Compositions of HIMU, EM1, and EM2 from global trends between radiogenic isotopes and major elements in ocean island basalts. *Earth and Planetary Science Letters, 276*, 175–186.

Jaramillo, C., Ochoa, D., Contreras, L., Pagani, M., Carvajal-Ortiz, H., Pratt, L. M., Krishnan, S., Cardona, A., Romero, M., & Quiroz, L. (2010). Effects of rapid global warming at the Paleocene-Eocene boundary on neotropical vegetation. *Science, 330*, 957–961.

Kerr, A. (2005). Oceanic LIPs: the kiss of death. *Elements, 1*, 289–292.

Kerr, A., White, R. V., Thompson, P. M. E., Tarney, J., & Saunders, A. (2003). No oceanic plateau - no caribbean plate? *The Seminal Role of an Oceanic Plateau in Caribbean Plate Evolution*, 126–168.

Kerr, A. C. (2014). Oceanic plateaus. In R. L. Rudnick (Ed.), *The crust* (pp. 631–667). Elsevier.

Kerr, A. C., & Mahoney, J. J. (2007). Oceanic plateaus: Problematic plumes, potential paradigms. *Chemical Geology, 241*, 332–353.

Kleibacker, D. W. (2001). *Sequence stratigraphy and lithofacies of the middle Eocene upper McIntosh and Cowlitz Formations, geology of the Grays River Volcanics, Castle Rock - Germany Creek area, southwest Washington* Unpublished MSc thesis. Oregon State University.

Klemme, S., & O'Neill, H. S. (2000). The near-solidus transition from garnet lherzolite to spinel lherzolite. *Contributions to Mineralogy and Petrology, 138*, 237–248.

Kushiro, I. (1996). Partial melting of fertile mantle peridotite at high pressures: an experimental study using aggregates of diamond. *Geophysical Monograph-American Geophysical Union, 95*, 109–122.

LeBas, M. J., LeMaitre, R. W., Streckeisen, A., & Zanettin, B. (1986). A chemical classification of volcanic rocks based on the total alkali-silica diagram. *Journal of Petrology, 27*, 745–750.

Lee, C.-T. A., Luffi, P., Plank, T., Dalton, H., & Leeman, W. P. (2009). Constraints on the depths and temperatures of basaltic magma generation on Earth and other terrestrial planets using new thermobarometers for mafic magmas. *Earth and Planetary Science Letters, 279*, 20–33.

Mahoney, J., Storey, M., Duncan, R., Spencer, K., & Pringle, M. (1993). Geochemistry and age of the Ontong Java Plateau. *The mesozoic Pacific: Geology, tectonics, and volcanism, 77*, 233–261.

Manikyamba, C., & Kerrich, R. (2012). Eastern Dharwar Craton, India: continental lithosphere growth by accretion of diverse plume and arc terranes. *Geoscience Frontiers, 3*, 225–240.

Mark, D. F., Barfod, D., Stuart, F. M., & Imlach, J. (2009). The ARGUS multicollector noble gas mass spectrometer: Performance for 40Ar/39Ar geochronology. *Geochemistry, Geophysics, Geosystems, 10*.

McCrory, P. A., & Wilson, D. S. (2013). A kinematic model for the formation of the Siletz-Crescent forearc terrane by capture of coherent fragments of the Farallon and Resurrection plates. *Tectonics, 32*, 718–736.

McCutcheon, M. S. (2003). *Stratigraphy and sedimentology of the middle eocene Cowlitz Formation and adjacent sedimentary and volcanic units in the Longview-Kelso area, southwest Washington*. Oregon State University.

McDonough, W. F., & Sun, S. S. (1995). The composition of the Earth. *Chemical Geology, 120*, 223–253.

McInerney, F. A., & Wing, S. L. (2011). The Paleocene-Eocene thermal maximum: A perturbation of carbon cycle, climate, and biosphere with implications for the future. *Annual Review of Earth and Planetary Sciences, 39*, 489–516.

McKenzie, D., & Bickle, M. J. (1988). The volume and composition of melt generated by extension of the lithosphere. *Journal of Petrology, 29*, 625–679.

McKenzie, D., & O'Nions, R. (1991). Partial melt distributions from inversion of rare earth element concentrations. *Journal of Petrology, 32*, 1021–1091.

Montelli, R., Nolet, G., Dahlen, F. A., & Masters, G. (2006). A catalogue of deep mantle plumes: New results from finite-frequency tomography. *Geochemistry, Geophysics, Geosystems, 7*.

Moothart, S. R. (1993). *Geology of the middle and upper Eocene McIntosh formation and adjacent volcanic and sedimentary rock units*. Willapa Hills, Pacific County, southwest Washington: Oregon State University.

Murphy, J. B., Hynes, A. J., Johnston, S. T., & Keppie, J. D. (2003). Reconstructing the ancestral Yellowstone plume from accreted seamounts and its relationship to flat-slab subduction. *Tectonophysics, 365*, 185–194.

Nelson, D. O., Morrison, D. A., & Phinney, W. C. (1990). Open-system evolution versus source control in basaltic magmas: Matachewan-Hearst dike swarm, Superior Province. *Canada. Canadian Journal of Earth Sciences, 27*, 767–793.

Nelson, P. L., & Grand, S. P. (2018). Lower-mantle plume beneath the Yellowstone hotspot revealed by core waves. *Nature Geoscience, 11*, 280–284.

Pearce, J. A. (1996). A user's guide to basalt discrimination diagrams. In D. Wyman (Ed.), *Trace element geochemistry of volcanic rocks: Application for massive sulphide exploration* (pp. 79–113). Mineral Deposits Division, Winnipeg: Geological Association of Canada.

Pearce, J. A. (2008). Geochemical fingerprinting of oceanic basalts with applications to ophiolite classification and the search for Archean oceanic crust. *Lithos, 100*, 14–48.

Peterson, D. W., & Moore, R. B. (1984). Geologic history and evolution of geologic concepts. *US Geological Survey Professional Paper, 1*, 149.

Phillips, B. A., Kerr, A. C., Mullen, E. K., & Weis, D. (2017). Oceanic mafic magmatism in the Siletz terrane, NW North America: Fragments of an Eocene oceanic plateau? *Lithos, 274-275*, 291–303.

Phillips, W., Walsh, T., & Mumford, D. (1989). Relationship between the Grays River volcanics of southwest Washington and the Tillamook volcanics of northwest Oregon. Eos. *Transations of the American Geophysical Union, 70*, 137.

Prestvik, T., & Goles, G. G. (1985). Comments on petrogeneses and the tectonic setting of Columbia River basalts. *Earth and Planetary Science Letters, 72*, 65–73.

Putirka, K. (2008). Excess temperatures at ocean islands: Implications for mantle layering and convection. *Geology, 36*, 283–286.

Pyle, D., Duncan, A. R., Wells, R., Graham, D. W., Hanan, B., Harrison, B., & Haileab, B. (2015). Longevity of Yellowstone hotspot volcanism: Isotopic evidence linking the Siletzia LIP (56 Ma) and early Columbia River Basalt Group (17 Ma) mantle sources. *AGU fall meeting*.

Pyle, D. G., Duncan, R., Wells, R., Graham, D., Harrison, B., & Hanan, B. (2009). Siletzia: An oceanic large igneous province in the Pacific Northwest. *Geological Society of America Abstracts with Programs*, 369.

Rarey, P. J. (1985). *Geology of the Hamlet-North Fork of the Nehalem River area, southern Clatsop and northernmost Tillamook Counties, northwest Oregon*. Oregon State University.

Renne, P. R., Balco, G., Ludwig, K. R., Mundil, R., & Min, K. (2011). Response to the comment by W.H. Schwarz et al. on "Joint determination of 40K decay constants and 40Ar*/40K for the Fish Canyon sanidine standard, and improved accuracy for 40Ar/39Ar geochronology" by P.R. Renne et al. (2010). *Geochimica et Cosmochimica Acta, 75*, 5097–5100.

Richter, F. M. (1988). A major change in the thermal state of the earth at the Archean-Proterozoic boundary: Consequences for the nature and preservation of continental lithosphere. *Journal of Petrology Special Volume*, 39–52.

Rudnick, R. L., & Fountain, D. M. (1995). Nature and composition of the continental crust: A lower crustal perspective. *Reviews of Geophysics, 33*, 267–309.

Saunders, A. D. (2015). Two LIPs and two earth-system crises: The impact of the North Atlantic igneous province and the Siberian traps on the earth-surface carbon cycle. *Geological Magazine, 153*, 201–222.

Schutt, D. L., & Humphreys, E. D. (2004). P and S wave velocity and VP/VS in the wake of the Yellowstone hot spot. *Journal of Geophysical Research: Solid Earth, 109*.

Snavely, P. D., MacLeod, N. S., & Wagner, H. C. (1968). Tholeiitic and alkalic basalts of the Eocene Siletz River volcanics, Oregon coast range. *American Journal of Science, 266*, 454–481.

Song, X.-Y., Keays, R. R., Xiao, L., Qi, H.-W., & Ihlenfeld, C. (2009). Platinum-group element geochemistry of the continental flood basalts in the central Emeishan Large Igneous Province, SW China. *Chemical Geology, 262*, 246–261.

Sparks, R. S. J., Folkes, C. B., Humphreys, M. C. S., Barfod, D. N., Clavero, J., Sunagua, M. C., McNutt, S. R., & Pritchard, M. E. (2008). Uturuncu volcano, Bolivia: Volcanic unrest due to mid-crustal magma intrusion. *American Journal of Science, 308*, 727–769.

Sun, S. s., & McDonough, W. F. (1989). Chemical and isotopic systematics of oceanic basalts: Implications for mantle composition and processes. *Geological Society, London, Special Publications, 42*, 313–345.

Tetreault, J., & Buiter, S. (2014). Future accreted terranes: a compilation of island arcs, oceanic plateaus, submarine ridges, seamounts, and continental fragments. *Solid Earth, 5*, 1243–1275.

Timpa, S., Gillis, K. M., & Canil, D. (2005). Accretion-related metamorphism of the Metchosin igneous complex, southern Vancouver Island, British Columbia. *Canadian Journal of Earth Sciences, 42*, 1467–1479.

Trehu, A., Asudeh, I., Brocher, T., Luetgert, J., Mooney, W., Nabelek, J., & Nakamura, Y. (1994). Crustal architecture of the Cascadia forearc. *Science, 266*, 237–243.

Walter, M. J. (1998). Melting of garnet peridotite and the origin of komatiite and depleted lithosphere. *Journal of Petrology, 39*, 29–60.

Wells, R., Bukry, D., Friedman, R., Pyle, D., Duncan, R., Haeussler, P., & Wooden, J. (2014). Geologic history of Siletzia, a large igneous province in the Oregon and Washington coast range: Correlation to the geomagnetic polarity time scale and implications for a long-lived Yellowstone hotspot. *Geosphere, 10*, 692–719.

Wells, R., Engebretson, D., Snavely, P., Jr, & Coe, R. (1984). Cenozoic plate motions and the volcano-tectonic evolution of western Oregon and Washington. *Tectonics, 3*, 275–294.

Westerhold, T., Röhl, U., & Laskar, J. (2012). Time scale controversy: Accurate orbital calibration of the early Paleogene. *Geochemistry, Geophysics, Geosystems, 13*, 1–19.

Westerhold, T., Röhl, U., McCarren, H. K., & Zachos, J. C. (2009). Latest on the absolute age of the Paleocene–Eocene Thermal Maximum (PETM): New insights from exact stratigraphic position of key ash layers+ 19 and− 17. *Earth and Planetary Science Letters, 287*, 412–419.

Wolfe, C. J., Bjarnason, I. T., VanDecar, J. C., & Solomon, S. C. (1997). Seismic structure of the Iceland mantle plume. *Nature, 385*, 245–247.

Yorath, C. J., Sutherland Brown, A., & Massey, N. W. D. (1999). Lithoprobe, southern Vancouver Island, British Columbia: Geology. *Geological Survey of Canada*, 109–133.

Zachos, J., Pagani, M., Sloan, L., Thomas, E., & Billups, K. (2001). Trends, rhythms, and aberrations in global climate 65 Ma to present. *Science, 292*, 686–693.

Zeebe, R. E., Zachos, J. C., & Dickens, G. R. (2009). Carbon dioxide forcing alone insufficient to explain Palaeocene–Eocene thermal maximum warming. *Nature Geoscience, 2*, 576–580.

Zindler, A., & Hart, S. (1986). Chemical geodynamics. *Annual Review of Earth and Planetary Sciences, 14*, 493–571.